

## Ordering thermodynamics of surface and subsurface layers in the $\text{Ga}_{1-x}\text{In}_x\text{P}$ alloy

Roberto Osório,\* James E. Bernard, Sverre Froyen, and Alex Zunger

*National Renewable Energy Laboratory, Golden, Colorado 80401*

(Received 4 December 1991)

Although *bulk* III-V alloys exhibit phase separation, vapor-phase epitaxial growth of  $\text{Ga}_{0.5}\text{In}_{0.5}\text{P}/\text{GaAs}$  (001) at  $\approx 900$ – $1000$  K shows spontaneous ordering into the  $\langle 111 \rangle$ -oriented monolayer  $(\text{GaP})_1(\text{InP})_1$  superlattice (the “CuPt” structure). Only two superlattice directions ( $[\bar{1}\bar{1}1]$  and  $[\bar{1}1\bar{1}]$ , which define the  $\text{CuPt}_B$  variant) out of four possible are seen. Both  $[\bar{1}\bar{1}1]$  and  $[\bar{1}1\bar{1}]$  subvariants are observed on flat surfaces or when surface steps are perpendicular to the cation dimers. Ordering was seen also in nonstoichiometric (e.g.,  $\text{Ga}_{0.7}\text{In}_{0.3}\text{P}$ ) alloys. Previous total-energy calculations at  $T=0$  show that (i) phase separation is eliminated by the constraint that the alloy and its constituents are coherently matched to a substrate; (ii) the epitaxially stable chalcopyrite order is eliminated by surface reconstruction; (iii) surface reconstruction stabilizes the  $\text{CuPt}_B$  variant over the other structures. A relaxed but unreconstructed surface does not lead to any significant preference for ordering. Here we develop thermodynamic ( $T \neq 0$ ) calculations based on cluster-variation solutions to a configurational Hamiltonian whose interaction energies are fit to  $T=0$  total-energy calculations. This shows that (iv) significant  $\text{CuPt}_B$  ordering persists to  $\sim 1500$  K not only for the equimolar  $\text{Ga}_{0.5}\text{In}_{0.5}\text{P}$  alloy, but also at other compositions, e.g.,  $\text{Ga}_{0.7}\text{In}_{0.3}\text{P}$ ; (v) the cation-terminated surface couples to the fourth layer in such a way as to select the correct three-dimensional  $\text{CuPt}_B$  structure; (vi) once formed, the two-dimensional  $\text{CuPt}_B$  layers near the surface are remarkably stable towards atomic swaps; (vii) a flat surface leads to a sufficiently small coupling between cation layers so that either of the two  $\text{CuPt}_B$  variants can form. We conclude that the main features of the observed ordering can be explained as a *thermodynamically stable phase* at growth temperatures of either the surface or the first few subsurface layers, depending on how deeply into the alloy atomic mobilities remain sufficiently large.

### I. INTRODUCTION

Recently, many observations have been made of spontaneous long-range order in III-V semiconductor alloys of composition  $A_{0.5}^{\text{III}}B_{0.5}^{\text{III}}C^{\text{V}}$  and  $C^{\text{III}}A_{0.5}^{\text{V}}B_{0.5}^{\text{V}}$ .<sup>1–11</sup> The ordering patterns observed can be described as short-period  $(AC)_p/(BC)_p$  superlattices in orientation  $\mathbf{G}$  and repeat period  $p$ . They include (i) the CuAu-I structure ( $p = 1$ ,  $\mathbf{G} = [001]$ ) seen in  $\text{Al}_{0.5}\text{Ga}_{0.5}\text{As}$  (Ref. 1) and  $\text{In}_{0.5}\text{Ga}_{0.5}\text{As}/\text{InP}$ ,<sup>2,3</sup> (ii) the chalcopyrite structure ( $p = 2$ ,  $\mathbf{G} = [201]$ ) seen in  $\text{GaAs}_{0.5}\text{Sb}_{0.5}/\text{InP}$ ,<sup>4</sup> and (iii) the CuPt structure ( $p = 1$ ,  $\mathbf{G} = [111]$ ) seen in  $\text{Ga}_{0.5}\text{In}_{0.5}\text{P}/\text{GaAs}$ ,<sup>5</sup>  $\text{InAs}_{0.5}\text{Sb}_{0.5}/\text{InSb}$ ,<sup>6</sup>  $\text{Al}_{0.5}\text{In}_{0.5}\text{P}/\text{GaAs}$ ,<sup>7</sup>  $\text{Ga}_{0.5}\text{In}_{0.5}\text{As}/\text{InP}$ ,<sup>8</sup>  $\text{In}_{0.5}\text{Al}_{0.5}\text{As}/\text{InP}$ ,<sup>9</sup>  $\text{GaAs}_{0.5}\text{P}_{0.5}$ ,<sup>10</sup> and  $(\text{Al}_x\text{Ga}_{1-x})_y\text{In}_{1-y}\text{P}/\text{GaAs}$ .<sup>11</sup> These observations have created interest both in the ordering mechanism<sup>12–22</sup> and in the technologically attractive possibility of tuning alloy band gaps at fixed composition through ordering.<sup>5,23–27</sup> To clarify the origins of ordering, first-principles total-energy and phase-diagram calculations were initially conducted for (i) three-dimensional (3D) *bulk* ordered structures<sup>28–33</sup> and alloys,<sup>34</sup> and (ii) 3D *epitaxial* superlattices and alloys coherent with a substrate.<sup>35,36</sup> These calculations showed that, for alloys with lattice mismatch between the constituents, the  $T=0$  lowest-energy 3D *bulk* configuration corresponds to phase separation, followed by the chal-

copyrite structure and then the random alloy, with the energy of the CuPt structure being considerably higher still. Metastable chalcopyrite ordering was predicted<sup>34</sup> to occur below a critical temperature in the range 200–500 K (depending on the system). The lowest-energy 3D *epitaxial* structure is chalcopyrite, again with CuPt being considerably higher in energy. Since the observed<sup>5–11</sup> CuPt phase is not the ground state in any of these calculations, it was suggested<sup>37</sup> that this type of ordering could be driven by *surface thermodynamic* rather than bulk thermodynamic effects.

The importance of surface effects was recognized also by others: Suzuki, Gomyo, and Iijima<sup>12</sup> proposed that the size difference between  $A$  and  $B$  atoms could favor CuPt ordering at the (001) surface just because of atomic relaxation without reconstruction. In this context, it is important to note that the four  $\langle 111 \rangle$  crystalline directions (along which a CuPt structure can be grown), which are symmetry equivalent in the bulk, divide into two classes in the presence of a surface:  $\{[111], [\bar{1}\bar{1}1]\}$  (termed the  $\text{CuPt}_A$  variant) and  $\{[\bar{1}\bar{1}1], [\bar{1}1\bar{1}]\}$  (termed the  $\text{CuPt}_B$  variant). The model of Suzuki, Gomyo, and Iijima implies that mixed-cation alloys (e.g.,  $\text{Ga}_{0.5}\text{In}_{0.5}\text{P}$ ) give  $\text{CuPt}_B$  ordering while mixed-anion alloys (e.g.,  $\text{GaAs}_{0.5}\text{Sb}_{0.5}$ ) would give  $\text{CuPt}_A$  ordering. However, Murgatroyd, Norman, and Booker<sup>15</sup> and Chen, Jaw, and Stringfellow<sup>19</sup> have established conclusively that both

types of alloys exhibit the same variant ( $\text{CuPt}_B$ ). Furthermore, the total-energy calculations of Froyen and Zunger<sup>21</sup> showed that  $A$ - $B$  size differences are easily accommodated at the free unreconstructed surface by *all* ordered structures (through atomic relaxation perpendicular to the surface plane) so that size differences could not provide a selective driving force for ordering. Matsumura, Kuwano, and Oki<sup>16</sup> followed the suggestion of Suzuki, Gomyo, and Iijima and investigated the ground-state structures of a quasi-two-dimensional Ising Hamiltonian representing the *ideal* (i.e., unreconstructed) surface and its interactions with the underlying layers. They found that  $\text{CuPt}$  order can appear for a certain range of the ratio between second- and first-neighbor cation interactions. Use of realistic surface interaction values (see Sec. VIA below), however, shows that the  $\text{CuPt}$  structure is not the ground state in the model of Matsumura, Kuwano, and Oki and that no ordered phases at all occur at growth temperatures. Along similar lines, Boguslawski<sup>14</sup> calculated the surface energies of various relaxed but unreconstructed surfaces, again finding small energy differences. These conclusions pointed to the possible role of *surface reconstructions*.<sup>21,22</sup>

It is well known that the (001) surface of III-V compounds exhibits not only relaxation but also reconstruction.<sup>38,39</sup> The dominant feature is the formation of cation and anion dimers<sup>40</sup> that introduce new surface symmetries. In mixed-anion alloys (e.g.,  $\text{GaAs}_{0.5}\text{Sb}_{0.5}$ ) the  $\text{CuPt}_B$  variant requires dimers between unlike atoms (i.e., As-Sb) on anion-terminated surfaces, while the  $\text{CuPt}_A$  variant requires dimers between like atoms (i.e., As-As and Sb-Sb). Murgatroyd, Nor-

man, and Booker<sup>15</sup> suggested that ordering in mixed-anion alloys is related to an energetic preference at the surface for mixed (e.g., As-Sb) dimers. This would give the observed variant provided that the mixed dimers are oriented with the same sense. However, in mixed-cation alloys, the  $\text{CuPt}_B$  variant in cation-terminated surfaces requires dimers between *like atoms* (e.g., Ga-Ga and In-In), while the  $\text{CuPt}_A$  variant requires dimers between unlike atoms (e.g., Ga-In). Hence, the observed ordering of  $\text{Ga}_{0.5}\text{In}_{0.5}\text{P}$  cannot be explained by the mechanism proposed by Murgatroyd, Norman, and Booker.

Froyen and Zunger<sup>21</sup> investigated the energetics of surface reconstruction for both anion- and cation-terminated (001) surfaces of GaP, InP, and  $\text{Ga}_{0.5}\text{In}_{0.5}\text{P}$ . They found that, in addition to dimerization, the cation-terminated surfaces exhibited two other electronically driven reconstruction modes: First, pairs of neighboring dimers along the  $[1\bar{1}0]$  dimer rows buckle (i.e., relax in opposite directions perpendicular to the surface), creating rows of alternating "high" and "low" dimers. Second, the high dimer tilts in the  $[110]$  direction, becoming nonhorizontal [Fig. 1(b)]. For the fully covered cation-terminated surface, pure dimerization lowers enormously the surface energy (by  $\sim 600$  meV/surface atom), with little energy difference between different Ga/In configurations. However, when buckling and tilting are permitted, the energy is lowered further by  $\sim 100$  meV/surface atom and a clear energetic preference emerges for the two-dimensional (2D)  $\text{CuPt}$ -like configuration consistent with the observed 3D  $\text{CuPt}_B$  structure in  $\text{Ga}_{0.5}\text{In}_{0.5}\text{P}/\text{GaAs}$ . Pure dimerization<sup>15</sup> hence does not provide a driving force for  $\text{CuPt}$  surface ordering,

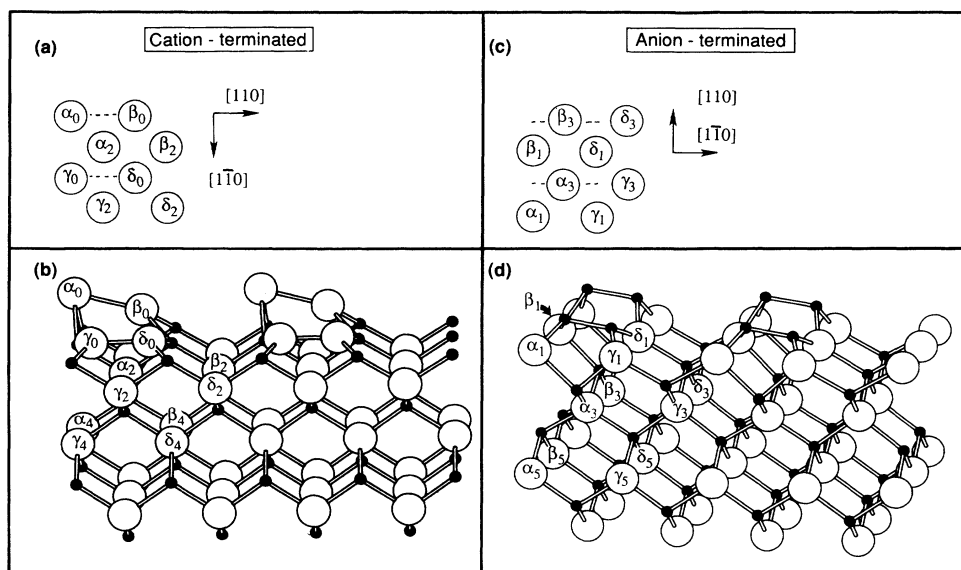


FIG. 1. Geometry of uppermost layers of (a) and (b) reconstructed, *cation-terminated*  $\text{Ga}_{0.5}\text{In}_{0.5}\text{P}$ ; and (c) and (d) reconstructed, *anion-terminated*  $\text{Ga}_{0.5}\text{In}_{0.5}\text{P}$ . Top views of ideal cation positions at the surface and in layers  $m = 1, 2$ , and  $3$  are given in (a) and (c). The dashed lines indicate the surface dimers. Side views are given in (b) and (d). Sublattices  $\alpha_m, \beta_m, \gamma_m$ , and  $\delta_m$  are indicated at each layer  $m$ . Cations are denoted by open circles and anions by solid circles.

but the combination of *dimerization, buckling, and tilting* does. Repeating the same calculation for the lattice-matched  $\text{Al}_{0.5}\text{Ga}_{0.5}\text{As}/\text{GaAs}$  (001) system revealed<sup>21</sup> no significant preference for any ordered structure, consistent with the fact that this system exhibits no ordering<sup>1</sup> on a (001) substrate at 50%-50% composition. For the anion-terminated  $\text{Ga}_{0.5}\text{In}_{0.5}\text{P}$  surfaces, buckling of dimer rows is also found, but the amount of buckling is smaller than for the cation-terminated surfaces, and the dimers remain nearly horizontal.

Ogale and Madhukar<sup>41</sup> have studied the adsorption of Ga and Al on a dimerized As-terminated (001) GaAs substrate using simulations based on semiempirical interaction potentials. They assumed simple, horizontal As-As dimers and neglected dimerization of the adsorbed cation pairs.<sup>22</sup> Their calculation revealed that anion dimerization induces specific site preferences for the adsorbed Ga and Al such that the top surface at 50%-50% composition takes up a 2D pattern at  $T=0$  consistent with the CuAu-I structure along [100] or [010] (or with the chalcopyrite structure along [201]). Simulations for a second mixed-cation layer, and for an additional As layer covering it, suggested that the three-dimensional stacking of these layers would form the CuAu-I structure. However, ordering is only observed in  $\text{Al}_{0.5}\text{Ga}_{0.5}\text{As}$  for a (110) substrate<sup>1</sup> on which dimerization does not occur. Further, this calculation gives no indication on the behavior expected for  $\text{Ga}_{0.5}\text{In}_{0.5}\text{P}$ , which was found<sup>21</sup> to differ substantially in surface energetics from  $\text{Al}_{0.5}\text{Ga}_{0.5}\text{As}$ .

Total-energy calculations for a single surface (or subsurface) layer alone are insufficient to determine whether the individual, surface-stabilized 2D CuPt layers of  $\text{Ga}_{0.5}\text{In}_{0.5}\text{P}$  will stack up in a correct 3D structure. Alternative possibilities are (i) the  $(\text{GaP})_2/(\text{InP})_2$  superlattice oriented along  $[1\bar{1}0]$ , in which the 2D CuPt-like layers stack differently than in bulk CuPt, and (ii) a disordered stacking of the 2D CuPt-like layers. This question of "phase locking" was recently addressed by Bellon *et al.*<sup>13</sup> and by Chen and Stringfellow.<sup>18</sup> Both groups suggested that surface steps may be involved in the preferential observation of one of the two possible ( $[1\bar{1}1]$  or  $[\bar{1}11]$ ) CuPt<sub>B</sub> subvariants. Both CuPt<sub>B</sub> subvariants are observed<sup>13,18</sup> on flat substrates or when surface steps are perpendicular to the cation dimers. It has been shown<sup>18</sup> that the presence of parallel steps can select one CuPt<sub>B</sub> subvariant over the other. Hamada and Kurimoto<sup>20</sup> showed that Ga is energetically favored over In immediately near a step at the plane below the step. Such a mechanism could provide correlations between nearest-neighbor cation layers, which could decide which of the two CuPt<sub>B</sub> subvariants is observed on vicinal (i.e., nonflat) substrates. However, the step model would need to include correlations in the [001] distribution of steps to account for the formation of the 3D CuPt<sub>B</sub> structure—rather than the  $(\text{GaP})_2/(\text{InP})_2$   $\mathbf{G} = [1\bar{1}0]$  superlattice or a disordered stacking of 2D CuPt<sub>B</sub>-like layers. It has become interesting, therefore, to investigate whether the presence of a reconstructed surface can exert an *energetic* preference for particular layer stackings. Bernard, Froyen, and Zunger<sup>22</sup> compared the elastic energy of various subsurface 2D structures and found an energetic preference for the correct

CuPt<sub>B</sub> stacking between the surface layer and the second cation layer below (four planes apart), even in the absence of surface steps.

A number of workers<sup>42,43</sup> have considered the possibility that the observed ordering does not correspond to a (local or global) minimum of the energy of either the bulk or the surface but that it represents instead a purely kinetic phenomenon. For example, having observed that nonstoichiometric (e.g.,  $\text{Ga}_{0.7}\text{In}_{0.3}\text{P}$ ) alloys show ordering,<sup>42</sup> Kondow *et al.* conjectured that this must reflect a kinetic product, since there is no known [111] ground-state structure with that composition. However, as we show below (Sec. VIB 3), a thermodynamic approach does produce CuPt<sub>B</sub> ordering at nonstoichiometric compositions. More recently, Chen and Khachaturyan<sup>43</sup> (CK) have considered systems whose ground state corresponds to phase separation (PS) but where a given ordered phase (*O*) can have lower energy than the homogeneous random alloy (*R*). A two-dimensional kinetic simulation of an Ising model with these properties then produced a temporal evolution exhibiting at finite times ordered domains ("virtual ordering") of type *O*. This was then offered as a possible mechanism for explaining ordering in III-V alloys. It had been previously shown,<sup>28,34,37</sup> however, that the energy sequence  $E(\text{PS}) < E(\text{O}) < E(\text{R})$  assumed by CK is present in lattice-mismatched III-V alloys only for the chalcopyrite ordering type *O*, which is not the one observed experimentally.<sup>5-11</sup> In this case, Wei, Ferreira, and Zunger<sup>34(b)</sup> showed that while metastable chalcopyrite ordering does exist, the ordering temperature is below growth temperatures. For the frequently observed ordering  $\text{O} = \text{CuPt}$ , the energy sequence is  $E(\text{PS}) < E(\text{R}) < E(\text{O})$ ,<sup>28,34,37</sup> so the CK model does not apply.

To summarize, previous calculations indicated that the energetics of (i) 3D bulk alloys, (ii) 3D epitaxial alloys, (iii) 2D relaxed surfaces, and (iv) 2D surfaces with simple dimerization cannot explain the observed *symmetry* of  $\text{Ga}_{1-x}\text{In}_x\text{P}$  ordering, while fully reconstructed 2D surfaces are consistent with observations but do not address the question of whether this ordering persists at finite temperatures or at nonstoichiometric compositions. While the slow diffusion of buried atoms certainly suggests that kinetics could play a role, kinetic models have not produced to date the correct symmetry for which ordering was actually seen.

The present study focuses therefore on the *finite-temperature* thermodynamics of the surface and subsurface layers in  $\text{Ga}_{1-x}\text{In}_x\text{P}/\text{GaAs}(001)$  at  $x = 1/2$  and  $x \neq 1/2$ . We use first-principles  $T = 0$  total-energy results<sup>21</sup> for the surface and first subsurface layers, as well as a large number of elastic energy calculations for various subsurface structures, to extract a realistic configurational Hamiltonian. The latter is formulated as a series of 2D layer Hamiltonians, each representing (with different parameters) the configurational energy of a surface or a given subsurface plane. The  $T=0$  ground-state structures of this Hamiltonian, as well as its  $T \neq 0$  thermodynamics, are then investigated.

Our major findings are the following. (i) As a consequence of reconstruction, the cation-terminated surface

orders in the  $\text{CuPt}_B$  structure and shows only a gradual decrease in the degree of order with temperature, *with no phase transition*. Indeed, a significant  $\text{CuPt}_B$  order parameter persists up to  $\sim 1500$  K not only in an equimolar  $\text{Ga}_{0.5}\text{In}_{0.5}\text{P}$  alloy, but also at other compositions, e.g.,  $\text{Ga}_{0.7}\text{In}_{0.3}\text{P}$ . This agrees with the experimental findings by Kondow *et al.*<sup>42</sup> (ii) Also as a consequence of reconstruction, the cation-terminated surface couples to the fourth subsurface layer in such a way as to select the correct 3D stacking of the 2D ordered  $\text{CuPt}_B$  structures in those layers. (iii) A study of the energies of intralayer atomic swaps shows a remarkable resilience of the two-dimensional  $\text{CuPt}$  structures at the surface of cation-terminated alloys and at the second cation subsurface layer of anion-terminated alloys. (iv) For the flat (i.e., no steps) surfaces studied here, the coupling between first-neighbor cation layers is very small, so that either of the two  $\text{CuPt}_B$  variants is free to form, as observed.

## II. METHODOLOGY: CONSTRUCTION OF CONFIGURATIONAL HAMILTONIAN FROM DIRECT TOTAL-ENERGY CALCULATIONS

Our first step is to construct a configurational cluster-expansion (CE) Hamiltonian  $\mathcal{H}_{\text{CE}}(\sigma)$  that describes the energy of the surface and subsurface  $\text{Ga}_{1-x}\text{In}_x\text{P}$  epitaxial layers in terms of a set of pseudospin variables

$$\sigma_i = \begin{cases} -1 & \text{for Ga} \\ 1 & \text{for In} \end{cases}, \quad (1)$$

describing the occupations of the cation sublattice sites  $i$ . (The common-anion sublattice is fully occupied by P.) The configuration vector  $\sigma$  describes the occupation of  $N$  cations in each of the  $n$  layers:  $\sigma = \{\sigma_1, \sigma_2, \dots, \sigma_{Nn}\}$ . The configurational Hamiltonian is expanded as a series of interaction energies  $\{J_F\}$  within various “figures”  $\{F\}$  (clusters of  $n_F$  sites):

$$\mathcal{H}_{\text{CE}}(\sigma) = N \sum_F D_F J_F \bar{\Pi}_F(\sigma), \quad (2)$$

where the degeneracy  $D_F$  is the number of symmetry-equivalent figures and  $\bar{\Pi}_F(\sigma)$  is the average spin product  $\frac{\sigma_i \sigma_j \dots \sigma_{n_F}}{n_F}$ . Such an Ising-like Hamiltonian is a convenient tool for (i) predicting the energy of configurations  $\sigma$  (not used in the fit), (ii) searching for  $T = 0$  ground-state structures (by direct constrained minimization), and (iii) calculating  $T \neq 0$  thermodynamic functions (by standard lattice statistics approximations such as the cluster-variation method).

Rather than design an *a priori* phenomenological configurational Hamiltonian,<sup>16,44</sup> we first perform a large set of *direct* total-energy calculations for many special 3D configurations  $\{\Sigma\}$ , and then identify the significant interaction energies that should enter the Hamiltonian  $\mathcal{H}_{\text{CE}}$ . For each configuration  $\Sigma$  we define from the directly (d) calculated total energy  $E_d(\Sigma)$ , the excess energy with respect to an equivalent mixture of phase-separated epitaxial  $\text{GaP/GaAs}$  and  $\text{InP/GaAs}$  slabs as

$$\Delta E_d(\Sigma) = E_d(\Sigma) - (1-x)E_d(\text{GaP}) - xE_d(\text{InP}). \quad (3)$$

These direct calculations are performed by a combination of *ab initio* pseudopotential and elastic valence-force-field (VFF) methods (see Sec. IV below). The  $n_{\text{CE}}$  parameters  $\{J_F\}$  of the cluster expansion (CE) are determined by projecting the set of  $n_d (\gg n_{\text{CE}})$  directly calculated energies into the CE by minimizing the error

$$\sum_{\Sigma} |\mathcal{H}_{\text{CE}}(\Sigma) - \Delta E_d(\Sigma)|^2. \quad (4)$$

In the final step, these interaction energies  $\{J_F\}$  are used in Eq. (2) to study the  $T \neq 0$  thermodynamics by means of the cluster-variation method.

## III. BASIC ASSUMPTIONS

We made the following basic assumptions in the present study.

### A. Neglect of surface segregation

Denote by  $(X, Y)$  the surface plane and by  $Z$  its normal direction. Many previous studies have focused on the  $Z$  dependence of  $(X, Y)$ -*averaged* quantities, such as composition.<sup>44–47</sup> These studies reveal segregation profiles along  $Z$ , but average over the internal structural degrees of freedom within the  $(X, Y)$  planes. Since the present study concerns ordering, we focus on the latter. Although segregation can occur in III-V alloys,<sup>47</sup> it is probably not a decisive factor in the ordering mechanism. Suppose that mobility is high enough to lead to an equilibrium situation in the upper  $m$  layers of the alloy and that it decreases abruptly so that it becomes negligible in deeper layers. The  $m$ th layer must then have the correct bulk stoichiometry before its mobility becomes negligible as a result of coverage by subsequent layers. The details of the interactions of the  $m$ th layer with upper layers may be influenced by composition variations of the upper layers. As we will see below, however, the crucial feature deciding the energetics of the deepest equilibrated layer is the presence of geometrically induced (“on-site”) interactions that are approximately independent of surface composition. We will therefore focus on the thermodynamic description of the particular forms of order of each  $(X, Y)$  plane at a given composition.

### B. Decoupling of geometric and topological degrees of freedom

There are two classes of positional degrees of freedom within the  $(X, Y)$  planes: (a) Layer *topology*, i.e., the discrete occupation variables of various *fixed* lattice sites in the  $(X, Y)$  plane by  $A$  and  $B$  atoms. A number of previous studies have focused on the statistics of the surface topology in alloys.<sup>16,17,44,48,49</sup> (b) Layer *geometry*, i.e., the continuous geometrical degrees of freedom available to the atoms with a fixed topology. The thermodynamics of dimerized surfaces of *elemental* semiconductors, with dimer-dimer “geometric” interactions was studied by Ihm

*et al.*<sup>50</sup> and Needels, Payne, and Joannopoulos.<sup>51</sup> Dimerization effects on subsurface layers have been discussed for the (IV-IV) Si-Ge alloy by Kelires and Tersoff.<sup>52</sup>

In our statistical model we assume that different cation-terminated surfaces retain similar equilibrium geometries for any topological occupation of the sites by *A* and *B* atoms. The assumed equilibrium geometry corresponds to the lowest-energy  $2 \times 2$  dimerized surface of  $\text{Ga}_{0.5}\text{In}_{0.5}\text{P}$  and is presented in Figs. 1(a) and 1(b) (for cation-terminated slabs) and Figs. 1(c) and 1(d) (for anion-terminated slabs). For both cation- and anion-terminated surfaces, total-energy pseudopotential calculations confirm that the lowest-energy  $2 \times 2$  surface geometry does not depend much on the site occupation.

To estimate the importance of defects in the dimer rows of Figs. 1(a) and 1(b), we have calculated by the first-principles pseudopotential method the energy for a  $2 \times 4$  geometrical structure consisting of two neighboring upper (In-In) dimers and two neighboring lower (Ga-Ga) dimers. The results indicate that the average energy of upper-upper and lower-lower dimer defects in a dimer row is  $\approx 320$  meV. Long rows of dimers in the  $2 \times 2$  geometry should therefore occur at growth temperatures ( $T \sim 900$  K) before any defects are created. There remains the question of what makes the dimer rows maintain their “correct” mutual position, so that upper dimers in one row stay close to upper dimers on a neighboring row. Our calculations show that sliding a row by one dimer with respect to a neighboring row results in an energy change of less than 20 meV/dimer. When multiplied by the average length of a perfect dimer row, however, the resulting effective row interaction is sufficiently high to maintain the  $2 \times 2$  geometry at growth temperatures. We hence deal in this paper with only the topological degrees of freedom in both the surface and subsurface layers.

### C. Assumption of fully covered surface

We assume a fully covered top surface. Pashley *et al.*<sup>38</sup> and Biegelsen *et al.*<sup>39</sup> observed scanning-tunneling-microscopy patterns of GaAs (001) surfaces that are consistent with *incomplete* As coverage. (A fully covered Ga surface in GaAs apparently has never been observed.) The calculations of Qian, Martin, and Chadi<sup>40</sup> indicate that a  $3/4$  monolayer coverage of As with a  $2 \times 4$  periodicity may have the minimum energy. There is, however, the possibility that a completely covered surface is stable in *other* semiconductors. In fact, pseudopotential total-energy calculations<sup>53</sup> have shown that, whereas fully covered GaAs and GaP cation-terminated surfaces are indeed unstable with respect to the formation of bulk metal, the reconstructed surfaces of InP and  $\text{Ga}_{0.5}\text{In}_{0.5}\text{P}$  are *stable at full coverage*. We will further assume that the reconstruction calculated at full coverage persists at the atmospheric pressures characteristic of metal-organic-chemical-vapor-deposition growth experiments.

### D. Independent-layer statistics

Whereas the full Hamiltonian includes intralayer and interlayer interactions, we describe in this study the thermodynamic properties of the surface and of each of the upper subsurface cation layers independently. This is justified for very thin (less than three cation layers)  $\text{Ga}_{0.5}\text{In}_{0.5}\text{P}$  slabs, since the interactions between  $x = 1/2$  cation planes are negligible for first-neighbor layer structures, although not negligible for some combinations of second-neighbor layer structures. Therefore, in principle the thermodynamics of upper layers should be supplemented by the contributions from interactions with deeper layers. However, we show in Secs. VI and VII below that the on-site terms in the cluster-expansion Hamiltonian [Eq. (2)] are responsible for ordering at growth temperatures in the upper layers of  $\text{Ga}_{1-x}\text{In}_x\text{P}$ . Interlayer interactions are small compared to the on-site energies.

## IV. DETAILS OF CALCULATION

Having described our basic methodology (Sec. II) and assumptions (Sec. III), we now describe the details of the calculation. The reader interested in the results can skip to Sec. V.

### A. Choice of 3D configurations for direct total-energy calculations

The set of special configurations  $\{\Sigma\}$  was obtained as follows: We first define as “building blocks” individual  $2 \times 2$  two-dimensional cation structures, with composition  $\text{Ga}_{1-x}\text{In}_x$  ( $x = 0, 1/2, \text{ and } 1$ ). Each of these 2D structures represents a different pattern of occupation of the sites of a (001) layer by Ga and In. The layer structures used here correspond to cross sections of the 3D  $\text{CuPt}_A$  ( $\text{CP}_A$ ),  $\text{CuPt}_B$  ( $\text{CP}_B$ ), and chalcopyrite (CH) ordered phases in addition to pure GaP and pure InP, used to define phase separation (PS). We call the 2D periodic structures  $\text{CP}_{A1}$ ,  $\text{CP}_{A2}$ ,  $\text{CP}_{B1}$ ,  $\text{CP}_{B2}$ ,  $\text{CH}_1$ ,  $\text{CH}_2$ ,  $\text{PS}_1$ , and  $\text{PS}_2$ . The unit cell for each of these 2D structures is displayed in the heading of Table I with respect to the geometric unit cell  $\alpha_m\text{-}\beta_m\text{-}\gamma_m\text{-}\delta_m$  of Fig. 1. Sublattices  $\alpha_m$ ,  $\beta_m$ ,  $\gamma_m$  and  $\delta_m$  are defined in Fig. 1 for each layer *m* by the position of their sites with respect to the four nonequivalent reconstructed-surface sites. The geometry of a layer  $m > 4$  is the same as that of layer  $m - 4$ . The geometries of subsurface layers are taken to be independent of their topologies, as is the geometry of the surface.

We then create the 3D structures  $\{\Sigma\}$  by stacking these 2D layers in different combinations. For example, the two 3D subvariants of  $\text{CuPt}_B$  are obtained by the stacking sequences  $\{B2, B2, B1, B1, \dots\}$  and  $\{B2, B1, B1, B2, \dots\}$ . The sequences  $\{B2, B2, B2, B2, \dots\}$  and  $\{B2, B1, B2, B1, \dots\}$  correspond to the  $(\text{GaP})_2(\text{InP})_2$  superlattice along  $[1\bar{1}0]$ . We have considered a total of 1449 3D configurations  $\Sigma$  for cation-terminated slabs with four  $\text{Ga}_{1-x}\text{In}_x\text{P}$  layers and an equal number for similar anion-terminated slabs.

TABLE I. Degeneracies  $D_F$  and average spin products  $\bar{\Pi}_F(m)$  for intralayers figures  $F$  (shown in Fig. 2) in the 2D structure shown on top of this table. The heading depicts the topological unit cell of each 2D structure (PS<sub>1</sub>-CH<sub>2</sub>) used in the fits, with respect to the  $\alpha_m$ - $\beta_m$ - $\gamma_m$ - $\delta_m$  geometric unit cell of Fig. 1. In these cells, the horizontal axis corresponds to the [110] direction and the vertical axis to  $[1\bar{1}0]$ . Open and solid circles denote Ga and In atoms, respectively. The columns denoted  $s_\alpha$ - $s_\delta$  display similar data for the  $x=1/4$  structures  $s_\mu$ . "Random" indicates the 2D random alloy. The average spin products for structures  $\bar{s}_\mu$  with  $x=3/4$  can be obtained from those for the complementary  $x=1/4$   $s_\mu$  structures by changing the signs of the  $\bar{\Pi}_F(m)$  corresponding to all  $\{\Delta J_i^j\}$ . Since only interactions within the same dimer row are considered,  $D_F=1/2$  for the  $m=0$  first-neighbor [110] pair (corresponding to  $J_2^{[110]}$ ) and  $D_F=1$  for second-neighbor pairs (corresponding to  $K_2$ ).

Figure	Interaction	$D_F$	2D structures												Random
			PS <sub>1</sub>	PS <sub>2</sub>	CP <sub>A1</sub>	CP <sub>A2</sub>	CP <sub>B1</sub>	CP <sub>B2</sub>	CH <sub>1</sub>	CH <sub>2</sub>	$s_\alpha$	$s_\beta$	$s_\gamma$	$s_\delta$	
Empty	$J_0$	1	1	1	1	1	1	1	1	1	1	1	1	1	1
Site $\alpha$	$\Delta J_1^\alpha$	1/4	-1	1	-1	1	-1	1	-1	1	1	-1	-1	-1	$2x-1$
Site $\beta$	$\Delta J_1^\beta$	1/4	-1	1	1	-1	-1	1	1	-1	-1	1	-1	-1	$2x-1$
Site $\gamma$	$\Delta J_1^\gamma$	1/4	-1	1	-1	1	1	-1	1	-1	-1	-1	1	-1	$2x-1$
Site $\delta$	$\Delta J_1^\delta$	1/4	-1	1	1	-1	1	-1	-1	1	-1	-1	-1	1	$2x-1$
First pair	$J_2^{[110]}$	1	1	1	-1	-1	1	1	-1	-1	0	0	0	0	$(2x-1)^2$
First pair	$J_2^{[1\bar{1}0]}$	1	1	1	1	1	-1	-1	-1	-1	0	0	0	0	$(2x-1)^2$
Second pair	$K_2$	2	1	1	-1	-1	-1	-1	1	1	0	0	0	0	$(2x-1)^2$

## B. Direct calculation of configurational energies

For each 3D structure  $\Sigma$ , we calculated the excess energy of Eq. (3) using the method described by Bernard, Froyen, and Zunger.<sup>22</sup> The basic principle involved is that, whereas the energy-minimizing geometry of the *top-surface* layer (exhibiting dimerization, buckling, and tilting) can be accurately determined only by minimizing the total *electronic* plus *elastic* energy [described here using the local-density approximation (LDA)], the geometry of "buried" subsurface layers represents largely the elastic response of atoms in these layers to the constraints placed on them by the structure of the top surface. Thus, for structures consisting of a monolayer of Ga<sub>0.5</sub>In<sub>0.5</sub>P on a GaAs substrate (the  $m=0$  and  $m=1$  cases), we calculate LDA total energies for reconstructed cation- and anion-terminated surfaces with each of the 2D layer structures. For thicker epilayers, we calculate the subsurface strain energies using an empirical VFF (Ref. 54) whose parameters were determined by fitting to LDA calculations. The energy of subsurface layers is minimized with respect to atomic relaxations using the conjugate-gradient method.<sup>55</sup> After averaging over the PS states in each layer, this gives a set of  $\approx 2900$   $\Delta E_d(\Sigma)$  values.

For the first-principles calculations, the accuracy of the differences between the energies for the various surfaces is estimated to be better than 10 meV/surface atom, based on a number of tests described in Refs. 21 and 22. The principal contribution to this error is from interactions between the two surfaces of the slab.

For the VFF calculations, there are three main sources of error: (i) the chemical energy necessarily omitted from an elastic-energy calculation, (ii) errors in the strain energy even in the bulk (e.g., anharmonic contributions), reflected in the inability to reproduce exactly strain energies calculated from first principles, and (iii) addi-

tional strain-energy errors induced by freezing the top two layers, omitting their strain energies, and using layer-independent VFF parameters for layers below the top two. The first of these is relatively small in this system, as is indicated by the fact that the difference between the VFF-predicted and the first-principles-predicted formation energies of bulk CuPt-ordered GaInP<sub>2</sub> [which includes errors of both type (i) and type (ii)] is about 2 meV/atom. The second of these we estimate to be of the order of 4 meV/atom, which represents both the maximum error in the strain energy of the binary compounds near equilibrium (relative to first-principles calculations) and the difference between the VFF-calculated and the first-principles-calculated energy differences between ideal and relaxed bulk CuPt-ordered GaInP<sub>2</sub>. The third source of error can be tested by determining the additional relaxation energy by VFF over what is found for the same slabs in the pseudopotential calculations. These energies can be relatively large (up to 140 meV/surface atom), but their average (over surfaces) can affect only the zeroth-order term in the cluster expansion that is fit to the VFF energies, and is therefore irrelevant. The variation of these relaxation energies with surface is generally less than 15 meV/surface atom (smaller for the cation-terminated surfaces). Because the cluster-expansion parameters are fit to the complete set of VFF results, they are effectively averaged out. Thus, the VFF errors relevant to the cluster expansion coefficients are limited to those in categories (i) and (ii) above (about 4 meV/atom).

## C. Results of direct calculation of configurational energies

We next describe the salient trends in these directly calculated energies, thus identifying the important inter-

TABLE II. Degeneracies  $D_F$  and average spin products  $\bar{\Pi}_F(m)$  for interlayer figures (shown in Fig. 3) connecting 2D structures at layer  $m \geq 4$  to 2D structures at layer  $m - 4$ .

Figure	Interaction	$D_F$	Pairs of 2D structures					
			$CP_{A1}/CP_{A1}$ $CP_{A2}/CP_{A2}$ $CP_{B1}/CP_{B1}$ $CP_{B2}/CP_{B2}$	$CP_{A1}/CP_{A2}$ $CP_{B1}/CP_{B2}$	$CH_1/CH_1$ $CH_2/CH_2$	$CH_1/CH_2$	$PS_1/PS_1$ $PS_2/PS_2$	$PS_1/PS_2$
Second pair	$K_2'$	1	1	-1	1	-1	1	-1
Third pair	$L_2'$	4	0	0	-1	1	1	-1
Fourth pair	$M_2'$	4	-1	1	1	-1	1	-1

actions that need to be described by a configurational Hamiltonian.

(a) The top cation surface shows a  $[110]$ - $[\bar{1}\bar{1}0]$  anisotropy (thus the energy of a  $CP_A$  structure at the top surface differs from that of a  $CP_B$ ) even without reconstruction. This occurs because surface cations are connected by anions immediately below only along the  $[\bar{1}\bar{1}0]$  direction.

(b) This anisotropy is enhanced by surface reconstruction. Pseudopotential calculations<sup>21,22</sup> for the energy of cation-terminated  $Ga_{0.5}In_{0.5}P$  surfaces with  $CP_A$ ,  $CP_B$ ,  $CH$ , and  $PS$  2D structures on (001) GaAs substrates (Table II of Ref. 22) indicate that the  $2 \times 2$  geometry of dimerized, buckled and tilted dimers [shown in our Fig. 1(b)] is preferred. Within that geometry, the  $CP_{B2}$  structure [see Table I and Fig. 1(a)], where two In atoms occupy the upper dimer, is energetically favored by 84 meV over the next-lowest-energy structure, namely,  $CH_1$ .

(c) For anion-terminated surfaces, reconstruction of the P atoms—with dimerization and buckling as shown in Fig. 1(d)—also lowers the energy.<sup>21</sup> However, the anion surfaces are still metallic; it is possible that a  $4 \times 2$  cell produces a lower-energy semiconducting surface.<sup>22</sup> Within the  $2 \times 2$  cell, the  $CH$  and  $CP_B$  structures of the first subsurface layer ( $m = 1$ ) [see Table I and Fig. 1(c)] have similar excess energies ( $\approx -30$  meV/atom).

(d) For the more deeply buried subsurface layers<sup>22</sup> ( $m \geq 2$ ), the ground state is  $CP_A$  for  $m = 2$  and  $CP_B$  for the  $m = 3$  and  $m = 4$  layers.

(e) For  $m \leq 4$ , the layer excess energy  $\Delta E_m(\Sigma_m)$  of the layer configuration  $\Sigma_m = \{\sigma_1, \sigma_2, \dots, \sigma_N\}$  is approximately independent (within a few meV) of the configurations of layers  $m' < m$ .<sup>22</sup>

(f) On the other hand, for  $m > 4$ ,  $\Delta E_m(\Sigma_m)$  depends significantly on the configuration of layer  $m - 4$  when two subvariants of the same pair (among the three pairs  $\{CP_{A1}, CP_{A2}\}$ ,  $\{CP_{B1}, CP_{B2}\}$ , and  $\{CH_1, CH_2\}$ ) occur in these layers.

(g) For layers  $m > 4$ , the average (with respect to different structures at  $m - 4$ ) ground state is one of the 2D  $CH$  structures. The lower-energy stacking of this 2D  $CH$  structure with respect to the two possible 2D  $CH$  structures at  $m - 4$  is consistent with the 3D chalcopyrite structure, which is the (epitaxially constrained) bulk ground state.

(h) On the other hand, the stacking of the two  $CP_A$  or  $CP_B$  variants has *higher* energy when it is consistent with the 3D CuPt structure, *except for*  $m = 4$ . In this case, if the surface layer is in its  $CP_B$  ground state, the energeti-

cally favored configuration of the  $m = 4$  layer is consistent with the correct stacking for the 3D CuPt structure.

#### D. The cluster expansion

Having established the main features of the directly calculated configuration dependence of  $\Delta E_d(\Sigma)$ , we now construct a finite-cluster-expansion Hamiltonian  $\mathcal{H}$  so that  $\mathcal{H}(\sigma)$  captures all salient features [(a)–(h) in the previous subsection (Sec. IV C)] of the directly calculated  $\Delta E_d(\Sigma)$ . We divide the Hamiltonian into intralayer and interlayer parts.

##### 1. Intralayer Hamiltonian

Like the total Hamiltonian of Eq. (2), the intralayer Hamiltonian that describes the excess energy of the layer configuration  $\sigma_m$  is expanded in a series of interactions  $J_F(m)$  associated with figures  $F$  at layer  $m$ ,

$$\mathcal{H}_m(\sigma_m) = N \sum_F D_F J_F(m) \bar{\Pi}_F(\sigma_m). \quad (5)$$

Note that, while all layers are described by the same figures  $\{F\}$ , the magnitude of the figure energy  $J_F(m)$  depends on the layer  $m$  at which the figure resides. In views of the trends found in the directly calculated energies (Sec. IV C), we design the terms in Eq. (5) as follows.

(i) The site-only figure of each sublattice  $\nu = \alpha, \beta, \gamma$ , and  $\delta$  is associated with the on-site energy  $\Delta J_1^\nu(m)$ . This describes the preferential occupation of sublattice  $\nu$  in each layer by Ga [if  $\Delta J_1^\nu(m) > 0$ ] or In [if  $\Delta J_1^\nu(m) < 0$ ]. These terms reflect the effects of local strains in a given subsurface layer induced there by the top-surface reconstruction and are responsible for features (b) and (d) of Sec. IV C. Only three of the four on-site energies are independent parameters: the on-site energies are constrained by the sum rule  $\sum_\nu \Delta J_1^\nu(m) = 0$ . Therefore, they do not lead to additional energy contributions in the  $x = 0$  and  $x = 1$  limits.

(ii) The first-neighbor pairs along the  $[110]$  and  $[\bar{1}\bar{1}0]$  directions are associated with interaction  $J_2^{[110]}(m)$  and  $J_2^{[\bar{1}\bar{1}0]}(m)$ , respectively, whereas the second-neighbor pairs (along  $[100]$  and  $[010]$ ), with interaction  $K_2(m)$ . These are shown in Fig. 2. These pair interactions describe corrections in the excess energy of each 2D layer configuration beyond the description given by on-site energies only. In particular, the pair interactions determine the preference for given 2D layer structures in layers

where, by symmetry, the on-site energies vanish (specifically, for  $m = 4n + 1$ , with  $n$  a non-negative integer). The intralayer pair interactions account for features (a), (c) and (g) (2D CH order) of Sec. IV C.

(iii) Finally, since the zero of energy was arbitrarily chosen to correspond to phase separation [Eq. (3)], a constant term  $J_0(m)$  is included to represent the excess energy per lattice site of a completely random  $x = 1/2$  layer [see Eq. (11) below].

The degeneracies  $D_F$  and average spin products  $\bar{\Pi}_F(\Sigma_m)$  for the eight 2D layer structures  $\Sigma_m$  are given in Table I along with those for the  $x = 1/4$   $2 \times 2$  structures. The intralayer cluster expansion becomes

$$\begin{aligned} \mathcal{H}_m(\sigma_m) = & N J_0(m) + \Delta J_1^\alpha(m) \sum_{i=1}^{N/4} \sigma_i + \Delta J_1^\beta(m) \sum_{j=1}^{N/4} \sigma_j + \Delta J_1^\gamma(m) \sum_{k=1}^{N/4} \sigma_k + \Delta J_1^\delta(m) \sum_{l=1}^{N/4} \sigma_l \\ & + J_2^{[110]}(m) \left( \sum_{\langle ij \rangle} \sigma_i \sigma_j + \sum_{\langle kl \rangle} \sigma_k \sigma_l \right) + J_2^{[1\bar{1}0]}(m) \left( \sum_{\langle ik \rangle'} \sigma_i \sigma_k + \sum_{\langle jl \rangle'} \sigma_j \sigma_l \right) \\ & + K_2(m) \left( \sum_{[il]} \sigma_i \sigma_l + \sum_{[jk]} \sigma_j \sigma_k \right), \end{aligned} \quad (6)$$

where  $i, j, k$ , and  $l$  denote sites on sublattices  $\alpha_m, \beta_m, \gamma_m$ , and  $\delta_m$ , indicated in Fig. 1,  $\langle \rangle$  and  $\langle \rangle'$  denote first-neighbor pairs along the  $[110]$  and the  $[1\bar{1}0]$  directions, respectively, and  $[ ]$  denotes second-neighbor pairs.

The on-site energies constitute the main symmetry-breaking effect of reconstruction introduced here. We neglect other smaller symmetry-breaking effects: for instance, an  $m = 1$  first-neighbor cation pair along the  $[1\bar{1}0]$  direction is described by the same interaction  $J_2^{[1\bar{1}0]}(1)$  regardless of whether the pair is located under a dimer row or under a trough between dimer rows [see Fig. 1(d)]. However, at the reconstructed surface, atoms along the  $[110]$  direction are assumed to interact [with intensity  $J_2^{[110]}(0)$ ] only when they belong to the same dimer [see Fig. 1(b)]. Similarly, surface second-neighbor interactions  $K_2(0)$  act only on pairs of atoms that belong to the same dimer row. For  $2 \times 2$  layer structures, this amounts to changing (for  $m = 0$ )  $J_2^{[110]}(m) \rightarrow J_2^{[110]}(0)/2$  and  $K_2(m) \rightarrow K_2(0)/2$  in Eq. (6).

## 2. Interlayer Hamiltonian

To understand features (e) and (f) (Sec. IV C) of the directly calculated energies, consider a more complete cluster expansion of a three-dimensional epitaxial pseudobinary alloy, grown on a (001) substrate, with the interactions indicated in Fig. 3. The constraint of fixed lattice constants in planes parallel to the substrate results in an anisotropy of otherwise equivalent interactions, e.g.,  $K_2 \neq K'_2$ . Interactions between first-neighbor cation lay-

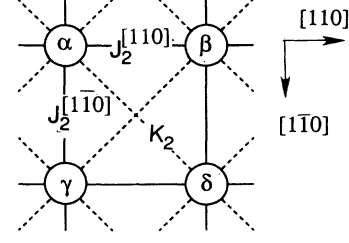


FIG. 2. Top view of intralayer figures used in the cluster expansion for the surface and subsurface layers of  $\text{Ga}_{1-x}\text{In}_x\text{P}$ . Only cations are shown.

ers ( $m$  and  $m - 2$ ) are given by  $J'_2$  and  $L_2$ , and those between second-neighbor cation layers ( $m$  and  $m - 4$ ), by  $K'_2, L'_2$  and  $M'_2$ .

The  $m/m - 2$  interlayer terms are

$$\mathcal{H}_{m,m-2} = J'_2 \sum_{\langle ij \rangle} \sigma_i \sigma_j + L_2 \sum_{\langle ik \rangle'} \sigma_i \sigma_k + J_4 \sum_{[ijkl]} \sigma_i \sigma_j \sigma_k \sigma_l, \quad (7)$$

where  $\langle ij \rangle$  denotes first-neighbor pairs and  $\langle ik \rangle'$  third-

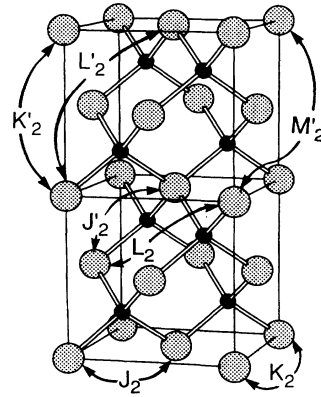


FIG. 3. Intralayer ( $J_2, K_2$ ) and interlayer cation-cation interactions between first-neighbor ( $J_2, L_2$ ) and second-neighbor ( $K_2, L_2, M_2$ ) layers in an epitaxial 3D pseudobinary alloy. The solid circles denote common atoms and the shaded circles denote mixed atoms.

neighbor pairs in which one of the sites belongs to layer  $m$  and the other to layer  $m - 2$ , and  $[ijkl]$  denotes first-neighbor tetrahedra in which two sites belong to layer  $m$  and the other two to layer  $m - 2$ . The  $m/m - 4$  interlayer terms are

$$\mathcal{H}_{m,m-4} = K'_2 \sum_{\{ij\}} \sigma_i \sigma_j + L'_2 \sum_{\{ik\}'} \sigma_i \sigma_k + M'_2 \sum_{\{il\}''} \sigma_i \sigma_l, \quad (8)$$

where  $\{ij\}$  denotes second-neighbor pairs,  $\{ik\}'$  third-neighbor pairs, and  $\{il\}''$  fourth-neighbor pairs in which one of the sites belongs to layer  $m$  and the other to layer  $m - 4$ .

The pair coefficients  $\bar{\Pi}_F(\Sigma)$  associated with  $\mathcal{H}_{m,m-2}$  are zero for structures  $\Sigma$  generated by the two-dimensional  $CP_A$ ,  $CP_B$ , CH, and PS structures. [Although the four-site  $\bar{\Pi}_F(\Sigma)$  coefficient is nonzero for some of the  $\{\Sigma\}$ , the fits show that contributions from  $J_4$  are insignificant.] This is just what is expected on the basis of symmetry:  $[110]$ - and  $[1\bar{1}0]$ -oriented pairs of sites in a  $2 \times 2$  cell in layer  $m - 2$  are symmetrically located with respect to the sites in layer  $m$ , thus precluding topological pair interactions that distinguish between configurations of a given composition in layer  $m - 2$ . This explains the near independence of these layer energies with respect to the next-layer configuration<sup>56</sup> [item (e) of Sec. IV C]. On the other hand, for  $\mathcal{H}_{m,m-4}$ , some pair  $\bar{\Pi}_F(\Sigma)$  coefficients for the  $2 \times 2$ ,  $x = 1/2$ , structures happen to be nonzero. These coefficients are given in the top part of Table II. This implies that the energy of  $m$ th layer configuration depends on the configuration of layer  $m - 4$ . Here it is also easy to see that such interactions are permitted by symmetry. Note (Table II) that the  $\bar{\Pi}_F(\Sigma)$  coefficients are nonzero for exactly the same pairs of structures at layers  $m$  and  $m - 4$  for which there is a significant correlation between VFF layer excess energies, as discussed in item (f) of Sec. IV C.

The total configurational Hamiltonian of a  $Ga_{1-x}In_xP$  slab with  $n$  cation layers is expressed as

$$\mathcal{H}_{CE} = \sum_m (\mathcal{H}_m + \mathcal{H}_{m,m-2} + \mathcal{H}_{m,m-4}), \quad (9)$$

where the intralayer term  $\mathcal{H}_m$  is given by Eq. (6) and the interlayer terms by Eqs. (7) and (8).

### E. Fitting the cluster expansion to directly calculated energies

The interaction parameters are determined by fitting the cluster expansion of Eqs. (6)–(8) to the set of directly calculated energies  $\{\Delta E_d(\Sigma)\}$ .

### 1. Fit of top-surface Hamiltonian

We extract surface interaction parameters from results obtained for a cation-terminated  $Ga_{0.5}In_{0.5}P$  monolayer on a GaAs substrate. The first line of Table III displays results obtained by mapping the cluster expansion for the top surface to pseudopotential calculations for the *unreconstructed* surface. Here, no *geometrical* preference exists for the occupation of each site by Ga or In. This occupation is then decided only by the *topological interactions* at the surface. This implies that each pair among  $\{CP_{A1}, CP_{A2}\}$ ,  $\{CP_{B1}, CP_{B2}\}$ , and  $\{CH_1, CH_2\}$  is made up of degenerate subvariants. As a result, the on-site energies  $\{\Delta J_1^\alpha(0)\}$  are zero and  $J_2^{[110]}(0)$ ,  $J_2^{[1\bar{1}0]}(0)$ , and  $K_2(0)$  are obtained by solving a  $3 \times 3$  system of linear equations [Eq. (5)].

The second line of Table III shows results for the *reconstructed* cation-terminated top surface. The topological degrees of freedom are now described by the Hamiltonian  $\mathcal{H}_0$  obtained from Eq. (6) (with  $m = 0$ ) including interactions only between atoms that belong to the same dimer row. Available to us are six *excess* energies  $\{\Delta E_d(\Sigma)\}$  calculated by the LDA pseudopotential method ( $CP_{A1}$ ,  $CP_{A2}$ ,  $CP_{B1}$ ,  $CP_{B2}$ ,  $CH_1$ , and  $CH_2$ , of Table I) and six interaction parameters [three of the  $\{\Delta J_1^\alpha(0)\}$  in addition to  $J_2^{[110]}(0)$ ,  $J_2^{[1\bar{1}0]}(0)$ , and  $K_2(0)$ ]. This leads to a well-determined  $6 \times 6$  system of linear equations [Eq. (5)], which is then solved for the interactions  $J_F(0)$ .

It is clear from Table III that the most important difference between the energetics of the reconstructed and the unreconstructed surfaces is described by the *on-site energies*: they are present only in the reconstructed case.

### 2. Fit of subsurface layer Hamiltonians

Table IV shows the results of fitting the  $m$ -dependent intralayer Hamiltonians of Eq. (6) and (for layers  $m \geq 4$ ) the interlayer Hamiltonians of Eqs. (7) and (8) to the directly calculated excess energies. The concentration of each layer is  $x = 0, 1/2$ , or 1. Since the top-surface geometry of cation-terminated alloys is different from that of anion-terminated alloys, and since these geometries exert different energy preferences for atomic configurations at deeper layers, we treat these two cases separately.

For cation-terminated alloys (even  $m$  in Table IV), we used 1449 different stackings of two-dimensional PS,  $CP_{A1}$ ,  $CP_{A2}$ ,  $CP_{B1}$ ,  $CP_{B2}$ ,  $CH_1$ , and  $CH_2$  structures in layers  $m = 0, 2, 4, 6$  in a slab of four  $Ga_{0.5}In_{0.5}P$  layers on a GaAs substrate. The Hamiltonian of Eqs. (6)–(8), with 27 interaction energies,<sup>57</sup> was then fitted by singular value decomposition<sup>58</sup> to the 1449 available directly

TABLE III. Intralayer interaction energies (in meV) for the *cation-terminated top surface* of  $Ga_{0.5}In_{0.5}P/GaAs$  (001) (see Fig. 2). Results are obtained from fits to pseudopotential calculations of unreconstructed and reconstructed surfaces.

Geometry	$J_0$	$\Delta J_1^\alpha$	$\Delta J_1^\beta$	$\Delta J_1^\gamma$	$\Delta J_1^\delta$	$J_2^{[110]}$	$J_2^{[1\bar{1}0]}$	$K_2$
Unreconstructed	1.8	0	0	0	0	-6.2	5.2	-0.4
Reconstructed	-2.3	-76	-100	90	86	-5.5	7.2	-2.2

TABLE IV. Intralayer interaction energies in layer  $m$ , and interlayer ( $m/m - 2$  and  $m/m - 4$ ) interaction energies (all in meV) for  $\text{Ga}_{0.5}\text{In}_{0.5}\text{P}/\text{GaAs}$ . Results for even  $m$  are for cation-terminated alloys while those for odd  $m$  are for anion-terminated alloys.  $J_4$  represents interactions between two sites on layer  $m$  and two sites on layer  $m - 4$ . The standard deviation is 2.5 meV for even  $m$  and 1.2 meV for odd  $m$ . In both cases, 27 independent parameters were fitted to 1449 directly calculated configurational energies. The corresponding epitaxial bulk parameters are also shown for comparison.

Layer $m$	Intralayer $m/m$						Interlayer $m/m - 2$ $m/m - 4$				
	$\Delta J_1^\alpha$	$\Delta J_1^\beta$	$\Delta J_1^\gamma$	$\Delta J_1^\delta$	$J_2^{[110]}$	$J_2^{[1\bar{1}0]}$	$K_2$	$J_4$	$K'_2$	$L'_2$	$M'_2$
0	-76.0	-100.0	90.0	86.0	-5.5	7.2	-2.2				
2	-51.6	51.6	-51.6	51.6	-11.3	-0.4	-4.6	-0.1			
4	23.4	35.2	-27.6	-30.9	2.7	3.2	-2.6	0.1	0.8	-0.7	0.5
6	-2.3	2.3	-2.3	2.3	2.4	2.8	-2.4	0.0	-6.6	-1.2	2.8
1	0.0	0.0	0.0	0.0	5.2	11.2	1.9				
3	104.9	104.9	-104.9	-104.9	3.1	2.8	-3.2	-0.1			
5	0.0	0.0	0.0	0.0	2.9	3.2	-2.4	0.1	-1.9	-0.7	1.2
7	-12.0	-12.0	12.0	12.0	2.4	2.8	-2.3	0.0	-5.0	-0.9	2.1
bulk	0.0	0.0	0.0	0.0	3.0	3.0	-2.6	0.0	-4.4	-0.9	2.0

calculated configurational energies  $\Delta E_d(\Sigma)$ , leading to a standard deviation of 2.5 meV. The geometry of the LDA-relaxed surfaces showed some breaking of the vertical mirror symmetry that would be expected at each dimer. This caused some splitting of the two  $\text{CP}_B$  subvariants at  $m = 2$ , for example. Since the symmetry breaking was small, and thought to be spurious (apparently being caused by residual interaction between the surfaces used in the pseudopotential calculations), it was removed from the surface geometries used in the VFF calculations from which the subsurface configurational Hamiltonian was obtained.

For the first subsurface layer ( $m = 1$ ) of an anion-terminated alloy, we neglected effects of the small tilting of P dimers and assumed no on-site energies. Pseudopotential results for the excess energy of  $\text{CP}_A$ ,  $\text{CP}_B$ , and CH structures of a  $\text{Ga}_{0.5}\text{In}_{0.5}\text{P}$  monolayer on a GaAs substrate are then used to obtain the values of  $J_2^{[110]}(1)$ ,  $J_2^{[1\bar{1}0]}(1)$  and  $K_2(1)$  displayed in Table IV.

For deeper layers of anion-terminated alloys (odd  $m$  in Table IV), we used 1449 similar combinations in layers  $m = 1, 3, 5, 7$  of an anion-terminated slab with four  $\text{Ga}_{0.5}\text{In}_{0.5}\text{P}$  layers. We assumed the dimerized but unbuckled surface geometry.<sup>59</sup> The fit of 27 interaction parameters to 1449 energies resulted in a standard deviation of only 1.2 meV. In order to better simulate the environment of the cation layer in the  $m = 7$  subsurface layer of a thicker  $\text{Ga}_{0.5}\text{In}_{0.5}\text{P}$  film, the top (As) layer of the substrate was changed to P. We have also fitted our Hamiltonian to directly calculated energies of anion-terminated slabs *without* the extra P layer: the results are similar (within 0.2 meV) to those shown in Table IV, except that  $J_2^{[110]}(7) = 3.1$  and  $J_2^{[1\bar{1}0]}(7) = -3.2$  meV. Without the extra P layer, the last-layer ( $m=7$ ) cations are connected by P atoms above (along the  $[110]$  direction) and by As (of the GaAs substrate) below (along the  $[1\bar{1}0]$  direction). The difference in size between Ga and As induces different  $J_2(7)$  contributions to the relaxation energy in the two directions. With the additional P layer,

this anisotropy is nearly removed.

The results obtained from the *surface* and *subsurface* fits are then compared to those obtained by fitting epitaxially constrained *bulk* VFF calculations. We used an anisotropic cluster expansion, where similar interaction parameters that represent different directions with respect to the substrate can assume different values (see Fig. 3). In Table IV “bulk” represents a six-parameter fit, including  $J_2 + 2L_2 = 0.41$  meV and the parameters  $J_2 \equiv J_2^{[110]} = J_2^{[1\bar{1}0]}$ ,  $K_2$ ,  $K'_2$ ,  $L'_2$ , and  $M'_2$  shown on the last line of Table IV. The six structures used were CuPt, CuAu  $[100]$ , CuAu  $[001]$ , chalcopyrite  $[201]$ , and the  $(\text{GaP})_2(\text{InP})_2$   $[001]$  and  $[110]$  superlattices. Note that the intralayer parameters for  $m > 2$  and the interlayer parameters between  $m=3$  and  $m=7$  approach the bulk results.

## V. RESULTS OF THE $T=0$ CLUSTER EXPANSION

### A. Configurational energies as a function of layer depth

Using Eq. (6) and the obtained intralayer interactions (Table IV), we plot in Fig. 4 the intralayer excess energy of the lower-energy subvariant of each pair  $\{\text{CP}_{A1}, \text{CP}_{A2}\}$ ,  $\{\text{CP}_{B1}, \text{CP}_{B2}\}$ , and  $\{\text{CH}_1, \text{CH}_2\}$  for layers  $m = 0, 1, \dots, 7$ . The energies displayed for each layer  $m$  correspond to averages over different stacking combinations of the 2D structures of the other layers ( $\neq m$ ). For comparison, we show the epitaxial bulk results, obtained by isolating the intralayer interactions in the epitaxial bulk fit. To illustrate the effect of interlayer interactions between second-neighbor cation layers we also plot the full epitaxial bulk results obtained from direct VFF calculations of (i) two superlattices with a common CP two-dimensional structure (CuPt and Y2, which is the  $(\text{GaP})_2(\text{InP})_2$  superlattice along  $[1\bar{1}0]$ ) and (ii) two superlattices with a common CH two-dimensional struc-

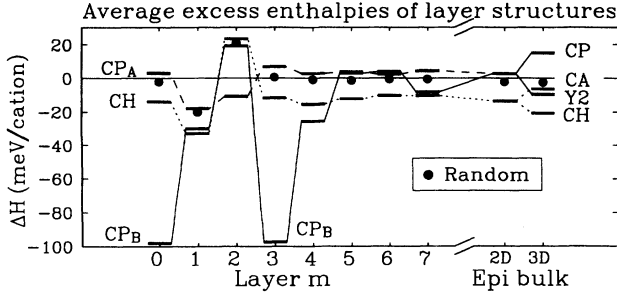


FIG. 4. The excess layer enthalpy (in meV/cation) at  $T = 0$  of several 2D structures and the 2D random alloy in  $\text{Ga}_{0.5}\text{In}_{0.5}\text{P}$  as function of the layer depth  $m$ . The zero of energy corresponds to phase separation at each layer. All energy values are averaged over different structures of other layers  $\neq m$ . Epitaxial bulk results using intralayer parameters only (“2D”) are also given, in comparison to the directly calculated epitaxial bulk structures (“3D”). Here Y2 represents the  $(\text{GaP})_2(\text{InP})_2$  superlattice along  $[1\bar{1}0]$  and CA represents the CuAu-I structure along  $[100]$ .

ture (CuAu  $[100]$  and chalcopyrite  $[201]$ ). The energy of the random configuration is obtained from the value of  $J_0$  in a 3D Hamiltonian analogous to Eq. (2).

Note in the bulk results in Fig. 4 that interlayer interactions stabilize the chalcopyrite structure but raise the energy of the CuPt structure. This is in agreement with the effect of interlayer interactions obtained from the cluster expansion [Eq. (8) and Tables II and IV] and also in agreement with the features of the VFF calculations described in items (f)–(h) of Sec. IV C. A comparison of different stackings of the two-dimensional  $\text{CP}_B$  structures shows that the interlayer terms in the cluster expansion [Eq. (8)] favor the Y2 structure over the three-dimensional CuPt<sub>B</sub> structure. It is important to realize, however, that the opposite signs of  $m=0$  and  $m=4$  on-site energies (Table IV) more than outweigh the effect of the interlayer terms and stabilize the correct CuPt<sub>B</sub> stacking between  $m=0$  and  $m=4$ .

### B. Predictions for atomic swaps and other compositions

The validity of the intralayer Hamiltonian of Eq. (6) can be further tested by its ability to predict the excess energies of new layer structures *not used in the fit*. Pseudopotential calculations of different atomic configurations in the surface are excessively computer intensive, but VFF calculations for subsurface-layer structures can be readily performed. We choose to test the ability of the model to predict the VFF energies of configurations at the third subsurface layer, the first to exhibit  $\text{CP}_B$  order. In the following, we compare CE and VFF calculations on (1)  $x = 1/2$  defect structures obtained by swapping first- or second-neighbor pairs of atoms in the third subsurface layer of the original structures used to fit the intralayer Hamiltonian and (2)  $x \neq 1/2$  third-subsurface-layer structures.

### 1. Atomic swaps

All intralayer first-neighbor and second-neighbor atomic swaps lead to a  $2 \times 2$  defect cell  $\mathbf{D}$  in one of the original  $2 \times 2$ -periodic structures  $\Sigma$ . We describe the host structure  $\Sigma$  by the spin variables  $\{\sigma_\nu\}$  in each of its four sublattices  $\{\nu\}$ :  $\Sigma = \{\sigma_\alpha, \sigma_\beta, \sigma_\gamma, \sigma_\delta\}$ . The defect is similarly described by the spin variables that define its four atoms:  $\mathbf{D} = \{d_\alpha, d_\beta, d_\gamma, d_\delta\}$ . Through an analysis of the defect-cell geometry of layers  $m \geq 1$ , we obtain the intralayer cluster expansion of the defect-cell excess energy (with respect to the original structure) in terms of the interaction energies of Eq. (6) and of the eight spin variables  $\{\sigma_\alpha, \sigma_\beta, \sigma_\gamma, \sigma_\delta, d_\alpha, d_\beta, d_\gamma, d_\delta\}$ . Using the model of  $2 \times \infty$  chains for the reconstructed surface, different expressions are obtained for interchain and intrachain defect cells at  $m=0$ .

Table V shows the predictions for defect energies  $\Delta E_{\Sigma;\mathbf{D}}$  as obtained by the cluster expansion compared with VFF results for swaps at the  $m = 3$  layer. The VFF results have been obtained for two layers of cation-terminated  $\text{Ga}_{0.5}\text{In}_{0.5}\text{P}$  with an additional phosphorus layer on top of the GaAs substrate. These results correspond to averages of  $m = 3$  defect energies for different  $m = 1$  layer structures (PS,  $\text{CP}_A$ ,  $\text{CP}_B$ , and CH). The cluster expansion predicts values of  $\Delta E_{\Sigma;\mathbf{D}}$  that are between 2 and 18 meV/(defect atom) higher than the VFF results, indicating that additional relaxations occur that partially relieve the strain at the defect-cell interface.

We also show in Table V the predictions of the cluster expansion for defect energies at  $m = 4$  and for interchain and intra-chain defect energies at  $m=0$ . The first five rows of Table V show that the  $\text{CP}_{B1}$  structure ex-

TABLE V. Predictions of the cluster expansion (CE) for the excess energies  $\Delta E_{\Sigma;\mathbf{D}}$  (in meV) of  $2 \times 2$  defect cells  $\mathbf{D}$  in the host structures  $\Sigma = \text{CP}_B$  and CH, for layers  $m=0, 3$ , and 4. We used the lower-energy subvariants of the indicated host structures (namely,  $\text{CP}_{B2}$  and  $\text{CH}_1$  for  $m=0$ ,  $\text{CP}_{B1}$  and  $\text{CH}_1$  or  $\text{CH}_2$  for  $m=3$ , and  $\text{CP}_{B1}$  and  $\text{CH}_2$  for  $m=4$ ). The notation  $\text{CP}_{B'}$  and  $\text{CH}'$  for the defect cells refers to the higher energy subvariants for each  $m$ . “Intra” and “inter” at  $m=0$  refer to defects inside a dimer row and between neighboring dimer rows, respectively. The predictions for  $m=3$  are compared to the directly calculated valence-force-field (VFF) results.

Host $\Sigma$	Defect $\mathbf{D}$	$m = 0$ (CE)		$m = 3$		$m = 4$ (CE)
		Intra	Inter	CE	VFF	
$\text{CP}_B$	$\text{CP}_{A1}$	395	386	378	370	100
	$\text{CP}_{A2}$	451	442	378	370	83
	$\text{CH}_1$	365	365	354	339	83
	$\text{CH}_2$	405	405	354	339	53
	$\text{CP}_{B'}$	744	770	758	743	177
CH	$\text{CP}_{A1}$	68	46	86	52	101
	$\text{CP}_{A2}$	124	102	86	52	84
	$\text{CP}_{B1}$	397	397	-332	-371	-27
	$\text{CP}_{B2}$	-307	-307	508	487	207
	$\text{CH}'$	116	90	125	52	139

hibits a remarkable resilience toward all first-neighbor and second-neighbor swaps at  $m=3$ . These swaps move a pair of Ga and In atoms to positions that require large local strain energies. In the description of the cluster expansion, such swaps require large on-site energies. We make a similar prediction of remarkable stability of the  $CP_{B2}$  layer structure at the top surface ( $m=0$ ) of a cation-terminated slab and, to a lesser extent, at the  $m=4$  layer. The fact that Ga/In swaps raise significantly the energy of the  $m=0$  (*surface*) and  $m=3$  (*subsurface*)  $CP_B$  cation layers of  $Ga_{0.5}In_{0.5}P$  (hence such swaps should not occur spontaneously) should be contrasted with the results for the *bulk*: Laks and Zunger<sup>60</sup> showed significant energy *lowering* for some swaps in the interior of the CuPt structure of  $Ga_{0.5}In_{0.5}P$ . On the other hand, the  $CH_2$  layer structure is stable in the interior of the epitaxially constrained  $Ga_{0.5}In_{0.5}P$  alloy,<sup>60</sup> but is unstable at  $m=3$  (Table V) against a nearest-neighbor swap that creates a  $CP_{B1}$  cell (and at  $m=0$  against a swap that creates a  $CP_{B2}$  cell). If atomic mobility is large enough at  $m=3$ , short-range swaps can therefore convert the  $CH_2$  structure into the  $CP_{B1}$  structure, which is stabilized by surface dimerization.

## 2. $x \neq 1/2$ structures

All compounds included in the fit correspond to layer compositions  $x=1/2$  or to layer phase separation. We analyze next the predictions of CE in comparison with

TABLE VI. Comparison of the predictions of the CE with directly calculated VFF results for (a) the excess energies (in meV/cation) of  $x=1/4$   $\{s_\nu\}$  and  $x=3/4$   $\{\bar{s}_\nu\}$  2D structures at  $m=3$  (first three columns) and (b) the excess energies of the structures of (a) superposed with structures of complementary composition ( $x=3/4$  and  $1/4$ ) at  $m=5$  (last three columns). Structure  $s_\nu$  ( $\bar{s}_\nu$ ) corresponds to In (Ga) in sublattice  $\nu$  and Ga (In) in the other three sublattices. For  $m=3$ , the pairs  $\{s_\alpha, s_\beta\}$  and  $\{s_\gamma, s_\delta\}$  are each made up of degenerate structures. For  $m=5$ , all four  $\{s_\nu\}$  structures are degenerate in the cluster expansion. The random configuration with  $x=1/4$  is denoted by  $R_{1/4}$  (degenerate with  $R_{3/4}$ ).

(a)			
$m=3$	CE	VFF	
$s_\alpha$	53.1	50.1	
$s_\gamma$	-51.8	-50.4	
$\bar{s}_\alpha$	-53.2	-56.4	
$\bar{s}_\gamma$	53.1	61.0	
$R_{1/4}$	0.5		
(b)			
$(m=3)/(m=5)$	CE	VFF	
$s_\alpha/\bar{s}_\nu$	51.7	48.6	
$s_\gamma/\bar{s}_\nu$	-53.2	-48.4	
$\bar{s}_\alpha/s_\nu$	-53.2	-56.4	
$\bar{s}_\gamma/s_\nu$	51.7	57.0	
$R_{1/4}/R_{3/4}$	0.1		

the VFF results for  $2 \times 2$  structures at compositions  $x=1/4$  and  $x=3/4$ . The cluster-expansion predictions can be readily obtained from Eq. (6) and Table I. As in Table I, we denote by  $s_\nu$  the  $x=1/4$  structure obtained by occupying the  $\nu$  sublattice by In and the others by Ga, and we denote by  $\bar{s}_\nu$  the  $x=3/4$  structure complementary to  $s_\nu$ .

Table VI(a) shows the CE and VFF results for the excess energy of these structures for  $m=3$ . The VFF results correspond to averages of these  $m=3$  two-dimensional structures with different  $m=1$  two-dimensional structures (PS,  $CP_A$ ,  $CP_B$ , and CH) immediately above, and a phosphorus layer and the GaAs substrate (at  $m=5$ ) immediately below. These energies are predicted by the CE with an error of  $< 8$  meV/cation.

Table VI(b) presents results for the excess energies of stackings of  $x=1/4$  and  $x=3/4$  structures at  $m=3$  and  $m=5$ , respectively, and for the complementary stackings of  $x=3/4$  and  $x=1/4$  structures. Again, the VFF results correspond to averages over different  $m=1$  two-dimensional structures immediately above, and a phosphorus layer and the GaAs substrate (at  $m=7$ ) immediately below. As in stackings of  $x=1/2$  layers, the interlayer terms of Eq. (7) do not contribute to the excess energy with respect to a concentration-weighted average of phase-separated layers. The CE errors are  $< 6$  meV/cation for the  $(m=3)/(m=5)$  stackings.

## VI. THERMODYNAMICS OF THE TOP SURFACE

Having established a mapping between a large set of directly calculated energies and a cluster expansion (Sec. IV E) and having tested its convergence and completeness at  $T=0$  (Sec. V B), we can now obtain the finite-temperature thermodynamics of the configurational Hamiltonian.

The thermodynamics of the unreconstructed and the  $2 \times 2$  reconstructed surfaces, with the interaction parameters of Table III, is obtained by minimizing the free energy  $F_0 = \mathcal{H}_0 - TS_0$  with respect to the average spin products  $\bar{\Pi}_F(\sigma)$ . For the unreconstructed surface we use the model of an anisotropic square lattice (equivalent to the rectangular lattice), while for the reconstructed surface we use the model of  $2 \times \infty$  independent rows. The square approximation of the cluster-variation method (CVM) (Ref. 61) was used to get the thermodynamics in both cases. This statistical treatment is described in the Appendix. The CVM approximation correctly takes into account the correlations inside the basic cluster (i.e., a square) and treats additional correlations in an approximate form that is exact only for one-dimensional chains or quasi-1D rows of width not larger than the size of the basic cluster. When the CVM square approximation is applied to the ferromagnetic isotropic Ising square lattice, a critical temperature that is 6.9% above Onsager's<sup>62</sup> exact solution is obtained.

Previous studies<sup>49,63</sup> of alloy surface thermodynamics with a fixed geometry showed the following trends when bulk interactions are assumed at the surface of systems

that display a first-order transition: (i) the surface often starts to disorder at temperatures below the bulk transition temperature,<sup>63</sup> but (ii) frustrated systems (e.g., the fcc lattice with antiferromagnetic interactions) can show a higher critical temperature at surfaces [like the (001)] where interactions are not frustrated.<sup>49</sup> Since interactions that lead to a chalcopyrite ground state are antiferromagnetic (and therefore frustrated) for first neighbors, the (001) (nonfrustrated)  $\text{Ga}_{0.5}\text{In}_{0.5}\text{P}$  surface is expected to exhibit chalcopyrite ordering if the bulk interactions are valid at the surface. The observation of  $\text{CuPt}_B$  ordering, instead, suggests that bulk interactions are inappropriate to the description of the surface. Indeed our calculations show that, even without reconstruction, surface interaction energies are different from the bulk (compare the last line of Table IV with the first line of Table III) and that reconstruction modifies further these interactions (Table III).

### A. Thermodynamics of the unreconstructed cation-terminated top surface

Minimization of the Hamiltonian of Eq. (6) produces the  $T = 0$  ground-state energy as a function of composition  $x$  (Fig. 5). For the *unreconstructed* cation-

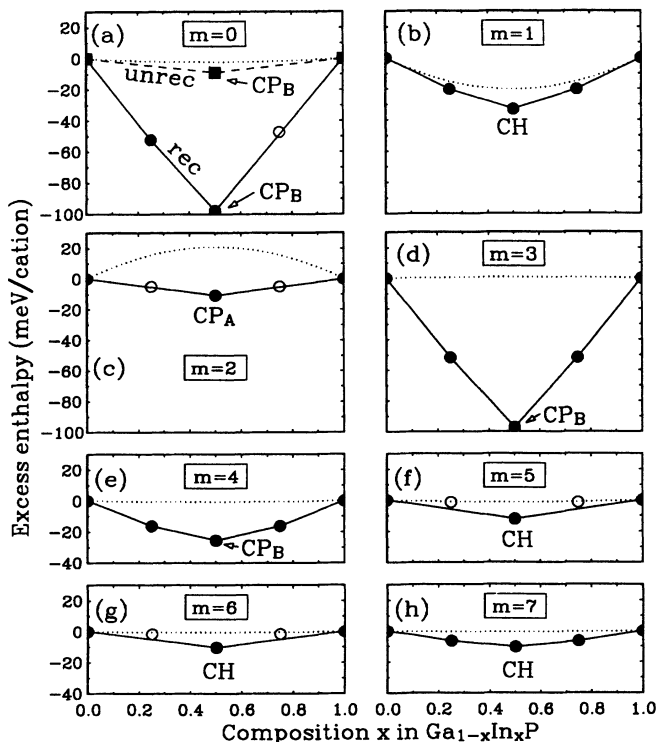


FIG. 5.  $T = 0$  ground-state structures for reconstructed 2D  $\text{Ga}_{1-x}\text{In}_x\text{P}$  at layer  $m$  below the surface. The ground-state structures are denoted by solid circles, indicating break points of broken lines. Open circles indicate lowest-energy single-phase structures at  $x = 1/4$  and  $3/4$  that are unstable with respect to phase separation. For comparison we show the energy of the random configuration (dotted lines) as functions of In composition  $x$ . The dashed line in (a) ( $m = 0$ ) gives the ground state of the unreconstructed surface.

terminated top surface [dashed line in Fig. 5(a)], we find that the  $\text{CP}_B$  structure is the ground state at  $x = 1/2$ . Phase separation occurs between pure GaP and  $\text{CP}_B$   $\text{Ga}_{0.5}\text{In}_{0.5}\text{P}$  in the interval  $0 < x < 1/2$  and between  $\text{CP}_B$   $\text{Ga}_{0.5}\text{In}_{0.5}\text{P}$  and InP in the interval  $1/2 < x < 1$ . To see if the energy differences between different surface structures are sufficient to preserve any type of order at typical growth temperatures, we calculated the order parameter  $\eta_B$ , defined as

$$\eta_B = \frac{1}{2} |c_\alpha + c_\beta - c_\gamma - c_\delta|, \quad (10)$$

as a function of temperature. Figure 6(a) displays the CVM results for the temperature dependence of  $\eta_B$  (dashed line) and of the In occupation probabilities  $c_\nu$  of the four sublattices  $\nu = \alpha, \beta, \gamma,$  and  $\delta$  in the unreconstructed cation-terminated surface. Note that  $\eta_B = 1$  at  $T = 0$  and  $\eta_B = 0$  after the system undergoes a phase transition to the disordered phase. We find a transition temperature  $T_c = 146$  K [Fig. 6(a)]. It is clear that at growth temperatures (typically 900 K) no traces of long-range  $\text{CP}_B$  ordering are to be expected in an unreconstructed surface.

Recently, Matsumura, Kuwano, and Oki (MKO) (Ref. 16) suggested a mechanism for spontaneous  $\text{CuPt}_B$  ordering of  $\text{Ga}_{0.5}\text{In}_{0.5}\text{P}$  alloys in terms of a layer-by-layer stacking sequence of (unreconstructed) minimum-energy layers. Application of our calculated interaction parameters for the unreconstructed surface (Table III) to the MKO model leads to the prediction that the  $(\text{GaP})_1/(\text{InP})_1$  superlattice along [001] (the  $\text{CuAu-I}$  structure) is the lowest-energy phase of the top surface, while the  $(\text{GaP})_2/(\text{InP})_2$  superlattice along  $[1\bar{1}0]$  (which has the same 2D structure as the  $\text{CuPt}_B$  phase), is the “ground-state-plane”<sup>16</sup> phase, which is defined as the lowest-energy phase of the first layer. However, since  $T_c$  ( $\sim 150$  K) is much lower than growth temperatures ( $\sim 900$  K), thermal disorder will lead to a vanishing order parameter at growth temperatures, as illustrated in Fig. 6(a). The MKO model is therefore unsuccessful in explaining the spontaneous  $\text{CP}_B$  ordering of  $\text{Ga}_{0.5}\text{In}_{0.5}\text{P}$  when realistic interactions are used.

### B. Thermodynamics of the reconstructed cation-terminated top surface

For the reconstructed-surface thermodynamics, correlations between the atomic occupations of different rows of cation dimers are expected to be small, since cations on different dimer rows are connected through at least three intermediate atoms. We thus use the *physical* approximation of  $2 \times \infty$  independent rows with a  $2 \times 2$  geometric unit cell that contains sites of the four sublattices  $\alpha_0, \beta_0, \gamma_0$  and  $\delta_0$  [see Fig. 1(a)]. For this physical approximation, the *mathematical* minimum-free-energy solution provided by the CVM square basic cluster (see Appendix) is *exact*, since the rows are uncorrelated and the system is quasi-one-dimensional. Besides, the order parameter of each chain obtained in this  $2 \times \infty$  model corresponds to an equivalent two-dimensional order parameter, since the chains are assumed to be positioned in phase in the geometry discussed in Sec. III B.

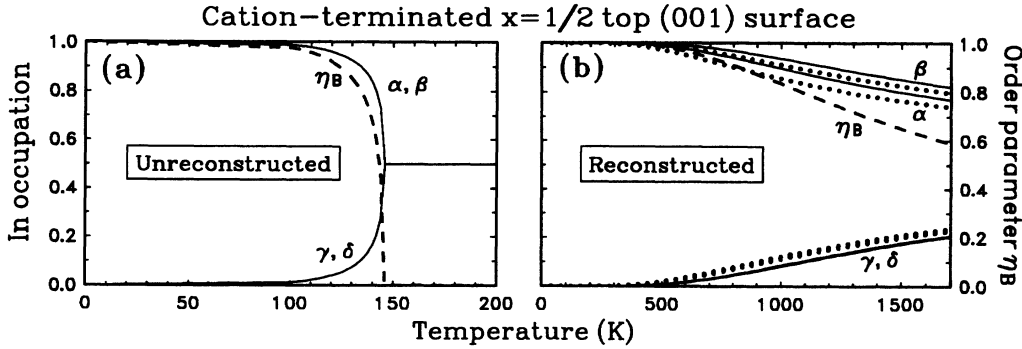


FIG. 6. Temperature dependence of the In occupation of sublattices  $\alpha$ ,  $\beta$ ,  $\gamma$ , and  $\delta$  at the top surface of (a) *unreconstructed* and (b) *reconstructed* cation-terminated Ga<sub>0.5</sub>In<sub>0.5</sub>P. The dotted curves in (b) indicate the predictions of a model with only on-site energies. The dashed curves in (a) and (b) indicate the CP<sub>B</sub> order parameter  $\eta_B$  [Eq. (10)], which goes to zero in (a) at  $T=146$  K.

### 1. Ground-state structures of the reconstructed top surface

The ( $T=0$ ) ground state was obtained by minimizing the intralayer Hamiltonian of Eq. (6) with the changes  $J_2^{[110]}(m) \rightarrow J_2^{[110]}(0)/2$  and  $K_2(m) \rightarrow K_2(0)/2$ , appropriate for reconstructed surfaces (see Sec. IV D 1). The solid line of Fig. 5(a) shows the predicted ground-state structures of the *reconstructed* cation-terminated Ga<sub>1-x</sub>In<sub>x</sub>P top surface ( $m=0$ ). The excess energies of the ordered structures  $s_\beta$  (at  $x=1/4$ ), CP<sub>B</sub> (at  $x=1/2$ ) and  $\overline{s}_\gamma$  (at  $x=3/4$ ) (defined in Table I) are indicated by circles. A common-tangent construction shows that the  $s_\beta$  structure is marginally *stable* against phase separation into pure GaP and CP<sub>B</sub>-like Ga<sub>0.5</sub>In<sub>0.5</sub>P; while the  $\overline{s}_\gamma$  structure is marginally *unstable* (or metastable) against phase separation into pure InP and CP<sub>B</sub>-like Ga<sub>0.5</sub>In<sub>0.5</sub>P. For comparison, the dotted line of Fig. 5(a) depicts the energy of the random surface alloy as a function of composition. The latter quantity was obtained by replacing the average spin products by their configurational averages  $\langle \sigma_i \rangle = 2x - 1$  (for all sublattices) and  $\langle \sigma_i \sigma_j \rangle = (2x - 1)^2$  (for all pairs). Since, by definition, the excess energy of the phase-separated system is zero, the excess energy of the random ( $R$ ) configuration (of any layer  $m$ ) becomes

$$\Delta E_R(m) = J_0[1 - (2x - 1)^2]. \quad (11)$$

For the top surface,  $J_0(0)$  is only  $-2.3$  meV (Table III) and the random configuration is therefore very close to phase separation for all  $x$ .

### 2. Thermal behavior of the $x=1/2$ top surface

Figure 6(b) shows the temperature dependence of the concentration  $c_\nu$  of In in the four different sublattices  $\nu$  of the reconstructed surface at composition  $x=1/2$ . Unlike the unreconstructed case of Fig. 6(a), *there is no phase transition*. The CP<sub>B</sub> order parameter  $\eta_B$  [Eq. (10)] is seen to be significant even at growth temperatures (e.g.,  $\eta_B \approx 0.83$  at  $T=1000$  K). This order parameter ap-

proaches zero only asymptotically as  $T \rightarrow \infty$ . To identify the interaction terms responsible for this behavior, we compare in Fig. 6(b) the predictions of the model with only on-site energies (dotted lines) to those obtained from the full layer Hamiltonian (full lines). Only a small difference in the order parameter of the two approximations is visible at  $T=1000$  K. Therefore, the stabilization of CP<sub>B</sub> order at growth temperatures can be understood as a pinning of the ordered structure by the on-site energies. These reflect the preference of (the larger) In atoms to occupy the upper dimer [ $\alpha_0$ - $\beta_0$  in Figs. 1(a) and 1(b)] and of (the smaller) Ga atoms to occupy the lower dimer ( $\gamma_0$ - $\delta_0$ ). Note, however [Fig. 6(b)] that within the upper dimer there is a slight preference of In atoms to occupy the lower site ( $\beta_0$ ) over the upper site ( $\alpha_0$ ). This is a result of the competition between size and electronegativity differences.<sup>21</sup> Comparison of Fig. 6(b) with Fig. 6(a) shows that reconstruction leads to the thermodynamic stabilization of a strongly ordered surface structure—consistent with the observed 3D CuPt<sub>B</sub> structure—at preparation temperatures.

### 3. The top surface of the $x=0.3$ alloy

Our model allows the prediction of the *finite-temperature* behavior of  $x \neq 1/2$  surfaces. Figure 7 shows the In occupation of the different sublattices for a Ga<sub>0.7</sub>In<sub>0.3</sub>P surface. It indicates a complete In occupation of the  $\beta_0$  sublattice and a 20% In occupation of the  $\alpha_0$  sublattice at  $T=0$ . Although these occupations are consistent with phase separation into 80%  $s_\beta$  (at  $x=1/4$ ) and 20% CP<sub>B2</sub> (at  $x=1/2$ ), a random distribution with the same 4:1 ratio of the two square-cluster configurations that are the unit cells for these structures (see heading of Table I) will have the same energy. (Since the other square-cluster configurations are not present, this state is partially ordered.) This single-phase state is the *stablest* at low nonzero temperatures. It corresponds to In on all  $\beta_0$  sites, Ga on all  $\gamma_0$  and  $\delta_0$  sites, and In and Ga randomly occupying the  $\alpha_0$  sites with concentrations 0.2 and 0.8, respectively.

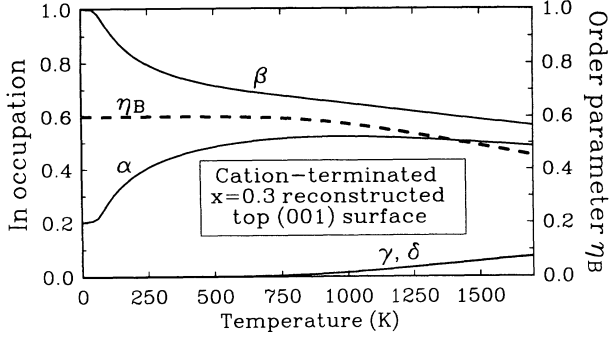


FIG. 7. Temperature dependence of the occupations of different sublattices in the reconstructed  $\text{Ga}_{0.7}\text{In}_{0.3}\text{P}$  cation-terminated top surface. The dashed curve indicates the  $\text{CP}_B$  order parameter  $\eta_B$  [Eq. (10)]. Full  $\text{CP}_B$  order ( $\eta_B=1$ ) would correspond to the In concentrations  $c_\alpha=c_\beta=1$  and  $c_\gamma=c_\delta=0$ .

Since

$$\Delta J_1^\alpha(0) - \Delta J_1^\beta(0) \ll \frac{1}{2} [\Delta J_1^\gamma(0) + \Delta J_1^\delta(0) - \Delta J_1^\alpha(0) - \Delta J_1^\beta(0)], \quad (12)$$

the In occupations of the  $\alpha_0$  and the  $\beta_0$  sublattices approach each other rapidly as the temperature increases, and characterize relatively strong two-dimensional  $\text{CP}_B$  order at  $T \approx 1000$  K. The result is consistent with the observation of  $\text{CuPt}_B$  ordering in these off-stoichiometry alloys.<sup>42</sup> The two-dimensional  $\text{CP}_B$  order parameter  $\eta_B$  is indicated by the dashed line in Fig. 7. Unlike the case where  $x=1/2$ , full  $\text{CP}_B$  order is not possible at  $x=0.3$ : thus  $\eta=0.6$  at  $T=0$  (as opposed to 1 for  $x=1/2$ ). Similarly to the  $x=1/2$  case,  $\eta \rightarrow 0$  asymptotically as  $T \rightarrow \infty$ .

## VII. THERMODYNAMICS OF SUBSURFACE LAYERS

### A. Calculation procedure

The temperature dependence of the occupation statistics of each subsurface layer is described by our intralayer Hamiltonian [Eq. (6)] with the parameters given in Table IV. We neglect interlayer interactions since corrections due to interlayer interactions would be of the same order of magnitude as those due to the introduction of intralayer interactions with respect to a model with on-site energies only [represented by dotted lines in Fig. 6(b)]. Such corrections would make the ground state at  $m=1$  and  $m \geq 5$  dependent on the configuration of the  $m-4$  and  $m+4$  layers, but would not change the state of order at  $T \approx 1000$  K for  $m=0, 2, 3, 4$ . For  $m=1$ , neglecting interlayer interactions is a good approximation for the case of a thin ( $x=1/2$ )  $\text{Ga}_{0.5}\text{In}_{0.5}\text{P}$  film of less than four layers, since [item (e) of Sec. IV C] the energy of  $x=1/2$  ordered structures is nearly independent of the atomic configuration of layers that are less than four layers (i.e., two cation layers) apart. The intralayer Hamiltonian is

solved in the CVM square approximation for each layer, as discussed in the Appendix.

### B. Ground-state structures of subsurface layers

Figures 5(b)–5(h) show the ground-state excess energies of layers  $m=1, 2, \dots, 7$ . At  $x=1/2$ , the ground state is  $\text{CP}_A$  for  $m=2$ ,  $\text{CP}_B$  for  $m=3$  and 4, and CH for  $m \geq 5$ . For comparison, we also show as dotted lines the energies of the random alloys [Eq. (11)]. Ground-state structures (circles in Fig. 5) are found at  $x=0, 1/4, 1/2, 3/4$ , and 1. They correspond to some of the  $x=1/4$  and  $x=1/2$  structures of Table I and to the  $x=3/4$  structures complementary to  $x=1/4$ . While the  $x=1/2$  ground state is usually well separated from other structures (except for  $m=1$ , where the CH ground state is very close in energy to the  $\text{CP}_B$  structure) the  $x=1/4$  and  $x=3/4$  ground states, in contrast, are considerably closer in energy to phase separation into  $x=0$  and  $x=1/2$  and into  $x=1/2$  and  $x=1$ , respectively.

### C. Thermal behavior at $x=1/2$

The temperature dependence of In sublattice occupations  $c_\nu$  is shown in Figs. 8(a)–8(c) for layers  $m=2, 3, 4$ ,

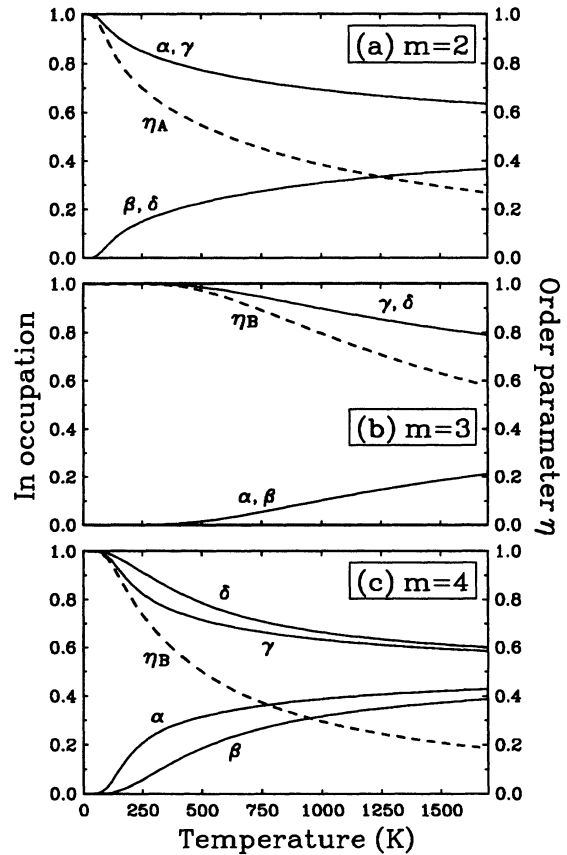


FIG. 8. Temperature dependence of the occupations of different sublattices at layers  $m=2, 3, 4$  in the reconstructed  $\text{Ga}_{0.5}\text{In}_{0.5}\text{P}$  alloy. The dashed curves indicate in (a) the  $\text{CP}_A$  order parameter  $\eta_A = (1/2)|c_\alpha + c_\gamma - c_\beta - c_\delta|$  and in (b) and (c) the  $\text{CP}_B$  order parameter  $\eta_B$  [Eq. (10)].

respectively. At typical preparation temperatures ( $T \sim 900$  K), the  $CP_B$  order parameter [Eq. (10)] is large at  $m=3$  and moderate at  $m=4$ . The  $m=2$  layer is strongly  $CP_A$  ordered at these temperatures. The  $m=1$  layer and layers with  $m > 4$  (not shown) are essentially disordered at preparation temperatures.

### VIII. EXTENT OF DIFFUSION AND ORDERING

The equilibrium ground state of an epitaxially-constrained three-dimensional  $Ga_{0.5}In_{0.5}P$  alloy is the chalcopyrite structure.<sup>36</sup> The observation of the  $CuPt_B$  structure shows that atomic mobilities are too low in the bulk of epitaxially grown alloys to promote bulk thermal equilibrium. The extent to which each layer equilibrium configuration influences the final 3D atomic configuration of the alloy depends on the rate of diffusion in different layers. It is also clear that surface reconstruction and the resulting on-site energies must play an important role in any scenario that could lead to 3D  $CuPt_B$  ordering. Our results indicate that scenario (i) of Bernard, Froyen, and Zunger<sup>22</sup> is a likely explanation for spontaneous growth of the observed  $CuPt_B$  structure on flat substrates at  $T \sim 900$  K. It consists of the following.

Suppose that the growing surface has cations exposed for a sufficiently long time so that reconstruction and surface  $CP_B$  ordering occurs, but diffusion is not sufficient to rearrange the state of order established at the surface after it is covered by additional layers. When a second layer is deposited, it will also order in the 2D  $CP_B$  structure, consistent with either the 3D  $CuPt_B$  structure or the  $(GaP)_2(InP)_2$  superlattice along  $[1\bar{1}0]$ . The third-layer stacking is the decisive factor in locking-in the 3D  $CuPt_B$  structure. The  $m=4$  on-site energies provide then an incentive for placing Ga at the top surface ( $m=0$ ) directly above In at the fourth subsurface layer ( $m=4$ ), as required for the correct stacking. Note that the  $m=4$  on-site energies in fact can be changed by moving only surface atoms, placing In atoms and their upper dimers preferentially over the Ga rows of  $m=4$ . Thus  $m=4$  on-site energies can determine the stacking sequence. The energy difference of  $\approx 60$  meV/surface atom that occurs between the two stacking possibilities of a  $CP_B$  surface structure must be multiplied by the average number of atoms in a dimer chain before defects—mainly two neighboring upper dimers or two neighboring lower dimers—occur. This therefore stabilizes considerably the correct 3D  $CuPt_B$  structure.

An alternative scenario can be proposed where the extent of diffusion is such that the  $m=3$  layer achieves its 2D  $CP_B$  stable state. The mechanism for correct 3D stacking is not clear in this case, since the results of our cluster expansion indicate that the stacking of 2D  $CP_B$  structures at the  $m=3$  and  $m=7$  layers has lower energy when it leads to the  $(GaP)_2/(InP)_2$   $G=[1\bar{1}0]$  superlattice than when it leads to the 3D  $CuPt_B$  structure.

### IX. CONCLUSIONS

A cluster expansion whose interaction energies are fitted to directly calculated energies of many configurations

of  $Ga_{1-x}In_xP/GaAs$  (001) leads to a useful description of the energetics of these structures and to the prediction of their thermodynamic behavior. The main results of this study are as follows.

(a) A two-dimensional  $CuPt_B$  order parameter—consistent with the observed spontaneous ordering in epitaxially grown  $Ga_{1-x}In_xP$ —corresponds to the thermodynamically stable phase for layers  $m=0, 3$ , and 4 at preparation temperatures. This occurs because the ground-state  $CuPt_B$  structures at these layers are pinned by reconstruction-induced local strains (on-site energies in the cluster expansion). Therefore, no phase transition occurs as the temperature increases. The order parameter decreases to zero only asymptotically as  $T \rightarrow \infty$ . Thus, in spite of relatively small energy differences between ordered structures at  $m=4$ , at  $T=1000$  K the  $CuPt_B$  (with the “correct” stacking sequence with respect to the surface) order parameter is still  $\approx 0.3$  (compared to 1 at  $T=0$ ). On-site energies at the surface sustain a strong surface ( $m=0$ )  $CuPt_B$  order parameter ( $\approx 0.8$ ) at  $T=1000$  K. For unreconstructed surfaces, on the other hand, where no on-site energies are present, the order parameter will be zero above  $T_c \approx 150$  K. We hence predict that “poisoning” reconstruction during growth will eliminate ordering.

(b) The observed  $CuPt_B$  ordering of (nonstoichiometric)  $Ga_{0.7}In_{0.3}P$  can also be explained as a surface thermodynamically stable phase at preparation temperatures.

(c) All Ga/In swaps between first- or second-neighbor atoms in the same plane raise the energy of two-dimensional  $x=1/2$  CuPt-like structures at the surface and at cation layers on the third and fourth subsurface (001) planes, although some of these swaps lower the energy in bulk CuPt-ordered structures.

(d) Ground-state structures as a function of composition are obtained for the surface and for several subsurface layers. For  $x=1/2$ , the energies of several two-dimensional structures as a function of the layer depth illustrate the evolution of the ground state from CuPt-like at the surface to chalcopyrite in the bulk.

### ACKNOWLEDGMENTS

This work was supported in part by the U.S. Department of Energy, Office of Energy Research, Basic Energy Science Grant No. DE-AC02-83CH10093.

### APPENDIX: THE STATISTICAL APPROXIMATION

The CVM square basic cluster<sup>61</sup> was used to obtain the thermodynamic properties of two models for  $Ga_{1-x}In_xP$  layers: (i)  $2 \times \infty$  chains were used as a model for the dimer chains at a reconstructed cation-terminated top surface and (ii) the anisotropic square lattice was used as a model for the unreconstructed surface and for subsurface layers in alloys with a reconstructed top surface. In case (i), the CVM square basic cluster provides an exact solution to the statistical-mechanical problem.

The CVM solution to a given lattice statistics problem consists of (i) expressing the excess energy  $\Delta E$  in terms of occupation variables, i.e., probabilities of different configurations of the CVM basic cluster and its subclusters, (ii) expressing the configurational entropy  $S$  of the lattice as an approximate function of the occupation variables, and (iii) minimizing the excess free energy  $\Delta F = \Delta E - TS$  with respect to the occupation variables for fixed external parameters such as temperature and concentration. Step (i) usually involves approximations inherent to the physical model employed, such as restricting the range of interactions to the size of the basic cluster. Step (ii) involves the fundamental mathematical approximation of CVM, and can be performed in a convenient way by the scheme proposed by Barker.<sup>64</sup> Statistical correlations within the basic cluster are described fully, but longer-range correlations are incorporated in a manner that is precise only for 1D systems (or quasi-1D systems—such as our  $2 \times \infty$  chains—whose width is not larger than the basic cluster). Step (iii) can be performed by a number of different numerical techniques (see, e.g., Ref. 55). It may be useful to describe the problem in terms of “correlation functions” (linear combinations of the occupation variables) by means of a “cluster algebra.”<sup>65</sup> The alternative simple scheme devised by Kikuchi<sup>66</sup> transforms the minimization problem into a system of coupled non-linear equations (on the occupation variables) that can be solved self-consistently. This “natural iteration” approach is used below in the two model systems analyzed here.

### 1. Exact solution to $2 \times \infty$ chains

The excess energy per site of  $2 \times \infty$  chains is expressed as

$$\Delta E = \sum_{a,b,c,d} \varepsilon_{abcd} z_{abcd}, \quad (\text{A1})$$

where  $a, b, c,$  and  $d$  denote spins  $\pm 1$  (representing In and Ga in  $\text{Ga}_{1-x}\text{In}_x\text{P}$ ), located on sublattices  $\alpha, \beta, \gamma,$  and  $\delta,$  respectively;  $\varepsilon_{abcd}$  represents the excess energy per site of configuration  $abcd$  of the basic square cluster; and  $z_{abcd}$  is the probability of occurrence of such a configuration. The spin products of Eq. (6) can be easily expressed as linear combinations of the  $\{z_{abcd}\}$ .

Using our Hamiltonian of Eq. (6), we write the basic cluster energies as

$$\begin{aligned} \varepsilon_{abcd} = & \frac{1}{4}[\Delta J_1^\alpha(0)a + \Delta J_1^\beta(0)b \\ & + \Delta J_1^\gamma(0)c + \Delta J_1^\delta(0)d] \\ & + \frac{1}{4}J_2^{[100]}(0)(ab + cd) + \frac{1}{2}J_2^{[0\bar{1}0]}(0)(ac + bd) \\ & + \frac{1}{2}K_2(0)(bc + da). \end{aligned} \quad (\text{A2})$$

We obtain the configurational entropy using Barker's scheme. This leads to

$$\begin{aligned} \frac{S}{Nk_B} = & -\frac{1}{2} \sum_{abcd} \mathcal{L}(z_{abcd}) \\ & + \frac{1}{4} \left( \sum_{ab} \mathcal{L}(y_{ab}^{\alpha\beta}) + \sum_{cd} \mathcal{L}(y_{cd}^{\gamma\delta}) \right), \end{aligned} \quad (\text{A3})$$

where  $\mathcal{L}(x) \equiv x(\ln x - 1)$ , and  $y_{ab}^{\alpha\beta}$  and  $y_{cd}^{\gamma\delta}$  denote occupation variables for the upper ( $\alpha\beta$ ) and lower ( $\gamma\delta$ ) dimers. These are related to the square cluster occupation variables by simple sum rules. A combinatorial argument similar to that used by Kikuchi<sup>61</sup> for the 1D lattice shows that the above expression gives the *exact* entropy per site  $S/(Nk_B) = (\ln G)/N$  of  $2 \times \infty$  chains, where  $G$  is the total number of possible arrangements of spins consistent with a given set of occupation variables  $\{z_{abcd}\}$ .

We add Lagrange multipliers  $\lambda_1$  and  $\lambda_2$  to the free energy to take into account constraints due to normalization of the square cluster occupation variables and due to a fixed In concentration  $x$ . The free energy then becomes

$$\begin{aligned} \Delta F = & \Delta E - TS - \lambda_1 \left( \sum z_{abcd} - 1 \right) \\ & - \lambda_2 \left( \sum z_{abcd} \frac{a+b+c+d}{4} - (2x - 1) \right). \end{aligned} \quad (\text{A4})$$

In the magnetic Ising problem, the parameter  $\lambda_2$  corresponds to the external magnetic field, which couples to the magnetization per site  $\sum z_{abcd}(a+b+c+d)/4$ .

Minimization of  $\Delta F$  in Eq. (A4) with respect to  $z_{abcd}$  gives

$$z_{abcd} = \exp\left(\frac{4\lambda_1 + (a+b+c+d)\lambda_2}{2k_B T}\right) z_{abcd}^{(0)}, \quad (\text{A5})$$

where

$$z_{abcd}^{(0)} = \exp\left(-\frac{2\varepsilon_{abcd}}{k_B T}\right) (y_{ab}^{\alpha\beta} y_{cd}^{\gamma\delta})^{1/2}. \quad (\text{A6})$$

If parameters  $\lambda_1$  and  $\lambda_2$  are known, Eqs. (A5) and (A6) can be solved self-consistently by iteration until a desired convergence criterion is satisfied. While  $\lambda_1$  is simply related to a normalization factor for  $z_{abcd}$ , determination of  $\lambda_2$  requires the solution of a fourth-degree polynomial in  $\rho \equiv \exp[\lambda_2/(k_B T)]$ , which results from applying the constant-composition constraint to Eqs. (A5) and (A6). This polynomial is solved for a positive  $\rho$  (and the resulting average of occupation variables checked to correspond to the given composition) at every iteration of Eqs. (A5) and (A6).

### 2. Approximate solution to the anisotropic square lattice

For the anisotropic square lattice model, the excess energy is given by Eq. (A1) with

$$\begin{aligned} \varepsilon_{abcd} = & \frac{1}{4}[\Delta J_1^\alpha(0)a + \Delta J_1^\beta(0)b \\ & + \Delta J_1^\gamma(0)c + \Delta J_1^\delta(0)d] \\ & + \frac{1}{2}J_2^{[100]}(0)(ab + cd) + \frac{1}{2}J_2^{[0\bar{1}0]}(0)(ac + bd) \\ & + K_2(0)(bc + da). \end{aligned} \quad (\text{A7})$$

Note the differences between Eqs. (A2) and (A7) due to the larger number of first-neighbor [100] and second-neighbor bonds when  $2 \times \infty$  chains are connected together to form the square lattice.

The entropy expression for the square lattice in the square cluster approximation is well known<sup>61</sup> and is expressed in our notation as

$$\begin{aligned} \frac{S}{Nk_B} = & - \sum_{abcd} \mathcal{L}(z_{abcd}) \\ & + \frac{1}{2} \left( \sum_{ab} \mathcal{L}(y_{ab}^{\alpha\beta}) + \sum_{cd} \mathcal{L}(y_{cd}^{\gamma\delta}) \right) \\ & + \sum_{ac} \mathcal{L}(y_{ac}^{\alpha\gamma}) + \sum_{bd} \mathcal{L}(y_{bd}^{\beta\delta}) \\ & - \frac{1}{4} \left( \sum_a \mathcal{L}(x_a^\alpha) + \sum_b \mathcal{L}(x_b^\beta) \right) \\ & + \sum_c \mathcal{L}(x_c^\gamma) + \sum_d \mathcal{L}(x_d^\delta) . \end{aligned} \quad (\text{A8})$$

Minimization of the free energy here leads to

$$z_{abcd} = \exp\left(\frac{4\lambda_1 + (a+b+c+d)\lambda_2}{4k_B T}\right) z_{abcd}^{(0)} , \quad (\text{A9})$$

where

$$z_{abcd}^{(0)} = \exp\left(-\frac{\varepsilon_{abcd}}{k_B T}\right) \frac{(y_{ab}^{\alpha\beta} y_{cd}^{\gamma\delta} y_{ac}^{\alpha\gamma} y_{bd}^{\beta\delta})^{1/2}}{(x_a^\alpha x_b^\beta x_c^\gamma x_d^\delta)^{1/4}} . \quad (\text{A10})$$

Equations (A9) and (A10) are solved by a procedure similar to that used in Sec. 1 of this Appendix for the  $2 \times \infty$  chains.

It is worth commenting on the accuracy of this solution to the intralayer Hamiltonian of Eq. (6). The CVM approach leads to exact results if only on-site energies are used in Eq. (6), since no correlations between squares are present in this case. (As a check, the on-site-energies-only results have been obtained independently by a Fermi-Dirac-like exact analysis and by the CVM program.) Therefore the errors in the statistics that is due to  $J_2$  and  $K_2$  interactions, e.g., the *difference* between the on-site-energies-only and the full-fit curves in Fig. 6(b). CVM thermodynamic functions, including order parameters and occupation variables, are usually very accurate at temperatures sufficiently far from a critical temperature (say  $|T - T_c| \gtrsim 0.2 T_c$ ).<sup>67</sup> Since phase transitions do not occur in the presence of large on-site energies, and since only the difference between the curves for the two fits is going to be affected by the CVM approximation, the CVM errors in the full-fit curves are expected to be very small.

\*Permanent address: Departamento de Física, Universidade de Brasília, 70910 Brasília, Distrito Federal, Brazil.

<sup>1</sup>T. S. Kuan, T. F. Kuech, W. I. Wang, and E. L. Wilkie, *Phys. Rev. Lett.* **54**, 201 (1985).

<sup>2</sup>T. S. Kuan, W. I. Wang, and E. L. Wilkie, *Appl. Phys. Lett.* **51**, 505 (1987).

<sup>3</sup>H. Nakayama and H. Fujita, in *GaAs and Related Compounds 1985*, Proceedings of the 12th International Symposium, Karuizawa, Japan, edited by M. Fujimoto, IOP Conf. Proc. No. 79 (Institute of Physics, Bristol, 1986), p. 289.

<sup>4</sup>H. R. Jen, M. J. Cherng, and G. B. Stringfellow, *J. Appl. Phys.* **48**, 1603 (1986); H. R. Jen, M. J. Jou, and G. B. Stringfellow, in *GaAs and Related Compounds 1986*, Proceedings of the 13th International Symposium, Las Vegas, edited by W. T. Lindley, IOP Conf. Proc. No. 83 (Institute of Physics, Bristol, 1987), p. 159; H. R. Jen, M. J. Jou, Y. T. Cherng, and G. B. Stringfellow, *J. Cryst. Growth* **85**, 175 (1987).

<sup>5</sup>A. Gomyo, T. Suzuki, and S. Iijima, *Phys. Rev. Lett.* **60**, 2645 (1988); T. Suzuki, A. Gomyo, S. Iijima, K. Kobayashi, S. Kawata, I. Hino, and T. Yuasa, *Jpn. J. Appl. Phys.* **27**, 2098 (1988).

<sup>6</sup>H. R. Jen, K. Y. Ma, and G. B. Stringfellow, *Appl. Phys. Lett.* **54**, 1154 (1989).

<sup>7</sup>M. Kondow, H. Kakibayashi, and S. Minagawa, *Phys. Rev. B* **40**, 1159 (1989).

<sup>8</sup>M. A. Shahid, S. Mahajan, D. E. Laughlin, and H. M. Cox, *Phys. Rev. Lett.* **58**, 2567 (1987); M. A. Shahid and S. Mahajan, *Phys. Rev. B* **38**, 1344 (1988); T. L. McDevitt, S. Mahajan, D. E. Laughlin, W. A. Bonner, and V. G. Keramidas, in *Epitaxial Structures*, edited by D. W. Shaw,

J. C. Bean, V. G. Keramidas, and P. S. Peercy (Materials Research Society, Pittsburgh, 1990), Vol. 198, p. 609.

<sup>9</sup>O. Ueda, T. Fujii, Y. Nakada, H. Yamada, and J. Umebu, *J. Cryst. Growth* **95**, 38 (1989).

<sup>10</sup>H. R. Jen, D. S. Cao, and G. B. Stringfellow, *Appl. Phys. Lett.* **54**, 1890 (1989); W. E. Plano, D. W. Nam, J. S. Major, K. C. Hsieh, and N. Holonyak, *ibid.* **53**, 2537 (1988).

<sup>11</sup>H. Okuda, C. Anayama, T. Tamahashi, and K. Nakejima, *Appl. Phys. Lett.* **55**, 2190 (1989).

<sup>12</sup>T. Suzuki, A. Gomyo, and S. Iijima, *J. Cryst. Growth* **93**, 396 (1988).

<sup>13</sup>P. Bellon, J. P. Chevalier, E. Augarde, J. P. André, and G. P. Martin, *J. Appl. Phys.* **66**, 2388 (1989).

<sup>14</sup>P. Boguslawski, *Phys. Rev. B* **42**, 3737 (1990).

<sup>15</sup>I. J. Murgatroyd, A. G. Norman, and G. R. Booker, *J. Appl. Phys.* **67**, 2310 (1990).

<sup>16</sup>S. Matsumura, N. Kuwano, and K. Oki, *Jpn. J. Appl. Phys.* **29**, 688 (1990).

<sup>17</sup>S. Matsumura, K. Takano, N. Kuwano, and K. Oki, *J. Cryst. Growth* **115**, 194 (1991); S. Matsumura, K. Takano, M. Ishimaru, N. Kuwano, and K. Oki (unpublished).

<sup>18</sup>G. S. Chen and G. B. Stringfellow, *Appl. Phys. Lett.* **59**, 324 (1991).

<sup>19</sup>G. S. Chen, D. H. Jaw, and G. B. Stringfellow, *J. Appl. Phys.* **69**, 4263 (1991).

<sup>20</sup>N. Hamada and T. Kurimoto, in *Proceedings of the 20th International Conference on the Physics of Semiconductors, Thessaloniki, 1990*, edited by E. M. Anastassakis and J. D. Joannopoulos (World Scientific, Singapore, 1990), p. 300.

<sup>21</sup>S. Froyen and A. Zunger, *Phys. Rev. Lett.* **66**, 2132 (1991);

- J. Vac. Sci. Technol. B **9**, 2176 (1991).
- <sup>22</sup>J. E. Bernard, S. Froyen, and A. Zunger, Phys. Rev. B **44**, 11 178 (1991).
- <sup>23</sup>A. Gomyo, K. Kobayashi, S. Kawata, I. Hino, T. Suzuki, and T. Yuasa, J. Cryst. Growth **77**, 367 (1986); A. Gomyo, T. Suzuki, K. Kobayashi, S. Kawata, I. Hino, and T. Yuasa, Appl. Phys. Lett. **50**, 673 (1987).
- <sup>24</sup>T. Nishino, Y. Inoue, Y. Hamakawa, M. Kondow, and S. Minagawa, Appl. Phys. Lett. **52**, 583 (1988).
- <sup>25</sup>S. Kurtz, J. Olson, and A. Kibbler, Solar Cells **24**, 307 (1988); Appl. Phys. Lett. **57**, 1922 (1990).
- <sup>26</sup>J. E. Bernard, S.-H. Wei, D. M. Wood, and A. Zunger, Appl. Phys. Lett. **52**, 311 (1988); S.-H. Wei and A. Zunger, J. Appl. Phys. **63**, 5794 (1988); Phys. Rev. B **39**, 3279 (1989); Appl. Phys. Lett. **53**, 2077 (1988); **56**, 662 (1990).
- <sup>27</sup>Y. Fu, K. A. Chao, and R. Osório, Phys. Rev. B **40**, 6417 (1989).
- <sup>28</sup>G. P. Srivastava, J. L. Martins, and A. Zunger, Phys. Rev. B **31**, 2561 (1985); **38** 12 984(E) (1988).
- <sup>29</sup>J. S. Nelson and J. P. Batra, Phys. Rev. B **39**, 3250 (1989).
- <sup>30</sup>P. Boguslawski and A. Baldereschi, Solid State Commun. **66**, 679 (1988); Phys. Rev. B **39**, 8055 (1989).
- <sup>31</sup>T. Ohno, Phys. Rev. B **38**, 13 191 (1988).
- <sup>32</sup>A. Qteish, N. Motta, and A. Balzarotti, Phys. Rev. B **39**, 5987 (1989).
- <sup>33</sup>D. M. Bylander and L. Kleinman, Phys. Rev. B **36**, 3229 (1987).
- <sup>34</sup>(a) L. G. Ferreira, S.-H. Wei, and A. Zunger, Phys. Rev. B **40**, 3197 (1989); (b) S.-H. Wei, L. G. Ferreira, and A. Zunger, *ibid.* **41**, 8240 (1990).
- <sup>35</sup>D. M. Wood and A. Zunger, Phys. Rev. Lett. **61**, 1501 (1988); Phys. Rev. B **40**, 4062 (1989); A. A. Mbaye, D. M. Wood, and A. Zunger, *ibid.* **37**, 3008 (1988); A. A. Mbaye, A. Zunger, and D. M. Wood, Appl. Phys. Lett. **49**, 782 (1986).
- <sup>36</sup>R. G. Dandrea, J. E. Bernard, S.-H. Wei, and A. Zunger, Phys. Rev. Lett. **64**, 36 (1990).
- <sup>37</sup>J. E. Bernard, L. G. Ferreira, S.-H. Wei, and A. Zunger, Phys. Rev. B **38**, 6338 (1988).
- <sup>38</sup>M. D. Pashley, K. W. Haberern, W. Friday, J. M. Woodal, and P. D. Kirchner, Phys. Rev. Lett. **21**, 2176 (1988); M. D. Pashley, Phys. Rev. B **40**, 10 481 (1989).
- <sup>39</sup>D. K. Biegelsen, R. D. Bringans, J. E. Northrup, and L.-E. Swartz, Phys. Rev. B **41**, 5701 (1990).
- <sup>40</sup>G.-X. Qian, R. M. Martin, and D. J. Chadi, Phys. Rev. B **38**, 7649 (1988).
- <sup>41</sup>S. B. Ogale and A. Madhukar, Appl. Phys. Lett. **59**, 1356 (1991).
- <sup>42</sup>M. Kondow, H. Kakibayashi, T. Tanaka, and S. Minagawa, Phys. Rev. Lett. **63**, 884 (1989).
- <sup>43</sup>L.-Q. Chen and A. G. Khachatryan, Phys. Rev. B **44**, 4681 (1991).
- <sup>44</sup>Y. Teraoka, Surf. Sci. Lett. **238**, L453 (1990); Surf. Sci. **242**, 113 (1991).
- <sup>45</sup>J. L. Morán-López, F. Mejía-Lira, and K. H. Bennemann, Phys. Rev. Lett. **54**, 1936 (1985).
- <sup>46</sup>R. S. Patrick, A.-B. Chen, A. Sher, and M. A. Berding, Phys. Rev. B **39**, 5980 (1989).
- <sup>47</sup>J. M. Moison, C. Guille, F. Houzay, F. Barthe, and M. Van Rompay, Phys. Rev. B **40**, 6149 (1989).
- <sup>48</sup>E. G. McRae, T. M. Buck, R. A. Malic, W. E. Wallace, and J. M. Sanchez, Surf. Sci. Lett. **238**, L481 (1990).
- <sup>49</sup>W. Schweika, K. Binder, and D. P. Landau, Phys. Rev. Lett. **65**, 3321 (1990).
- <sup>50</sup>J. Ihm, D. H. Lee, J. D. Joannopoulos, and J. J. Xiong, Phys. Rev. B **20**, 1872 (1983).
- <sup>51</sup>M. Needels, M. C. Payne, and J. D. Joannopoulos, Phys. Rev. B **38**, 5543 (1988).
- <sup>52</sup>P. C. Kelires and J. Tersoff, Phys. Rev. Lett. **63**, 1164 (1989).
- <sup>53</sup>S. Froyen and A. Zunger (unpublished).
- <sup>54</sup>P. N. Keating, Phys. Rev. **145**, 637 (1966).
- <sup>55</sup>W. H. Press, B. P. Flannery, S. A. Teukolsky, and W. T. Vetterling, *Numerical Recipes* (Cambridge University Press, Cambridge, 1986), pp. 301–306.
- <sup>56</sup>The dependence of the energies of an ordered  $x = 1/2$  cation layer on the structure of the next cation layer above it is only significant for  $m = 2$ . There the  $K'_2$  and  $L_2$  interactions between  $m = 2$  and  $m = 0$  are in fact split in four interactions each due to the pronounced displacement of the surface atoms from their equilibrium bulk positions and the model presented here is less precise. This is the main reason for a larger standard deviation (Sec. V B) for a cation-terminated slab than for an anion-terminated slab.
- <sup>57</sup>The fitted parameters are (a) the intralayer interactions  $J_2^{[110]}(m)$ ,  $J_2^{[110]}(m)$ ,  $K_2(m)$ , and three of the  $\{J_1^\gamma(m)\}$ , for  $m \geq 2$ , (b) the  $m/m - 2$  interaction  $J_4(m)$  for  $m \geq 2$ , and (c) the  $m/m - 4$  interactions  $K'_2(m)$ ,  $L'_2(m)$  and  $M'_2(m)$  for  $m \geq 4$ .
- <sup>58</sup>W. H. Press, B. P. Flannery, S. A. Teukolsky, and W. T. Vetterling, *Numerical Recipes* (Ref. 55), pp. 52–64.
- <sup>59</sup>For anion-terminated epilayers, the geometry of the LDA-relaxed surfaces includes a degree of symmetry-breaking dimer buckling. With buckled surfaces, we find that four distinct  $\{\Delta J_1^\gamma(m)\}$  are present at  $m = 3$  and  $m = 7$ , while if the buckling is removed  $\Delta J_1^\alpha(m) = \Delta J_1^\beta(m)$  and  $\Delta J_1^\gamma(m) = \Delta J_1^\delta(m)$ . Since the buckled surfaces are still metallic, they probably do not correspond to the lowest-energy geometry (that is, the surface unit cell used in the pseudopotential calculations is probably not large enough for the global energy minimum to be obtained). We thus choose to present results corresponding to the simpler dimerized, unbuckled geometry. Note that the strong  $CP_B$  ordering found at  $m = 3$  (Sec. V A) is a consequence of dimerization only and is present for both the buckled and unbuckled reconstructions. It should also be present in more complex reconstructions. A  $4 \times 2$  reconstruction, with three high dimers and one low dimer per unit cell, which could lead to a lower energy (Ref. 22), should thus also lead to a substantial  $CP_B$  order parameter at  $m = 3$ .
- <sup>60</sup>D. B. Laks and A. Zunger (unpublished).
- <sup>61</sup>R. Kikuchi, Phys. Rev. **81**, 988 (1951).
- <sup>62</sup>L. Onsager, Phys. Rev. **65**, 117 (1944).
- <sup>63</sup>R. Lipowsky, J. Appl. Phys. **55**, 2485 (1984).
- <sup>64</sup>J. A. Barker, Proc. R. Soc. London Ser. A **216**, 45 (1953).
- <sup>65</sup>J. M. Sanchez and D. de Fontaine, Phys. Rev. B **17**, 2926 (1978).
- <sup>66</sup>R. Kikuchi, J. Chem. Phys. **60**, 1071 (1974).
- <sup>67</sup>See, for instance, D. de Fontaine, in *Solid State Physics*, edited by H. Ehrenreich, F. Seitz, and D. Turnbull (Academic, New York, 1977), Vol. 34, p. 73.

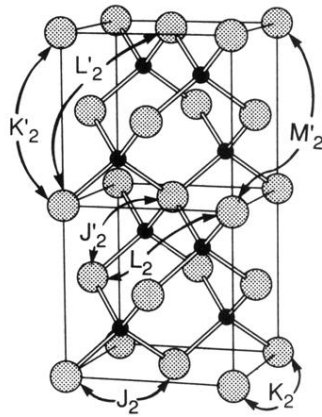


FIG. 3. Intralayer ( $J_2$ ,  $K_2$ ) and interlayer cation-cation interactions between first-neighbor ( $J'_2$ ,  $L_2$ ) and second-neighbor ( $K'_2$ ,  $L'_2$ ,  $M'_2$ ) layers in an epitaxial 3D pseudobinary alloy. The solid circles denote common atoms and the shaded circles denote mixed atoms.